

Nanosecond electro-optics of a nematic liquid crystal with negative dielectric anisotropyVolodymyr Borshch,^{1,*} Sergij V. Shiyankovskii,¹ Bing-Xiang Li,^{1,2} and Oleg D. Lavrentovich^{1,†}¹*Liquid Crystal Institute, Chemical Physics Interdisciplinary Program, Kent State University, Kent, Ohio 44242, USA*²*College of Electronic and Information Engineering, Nanjing University of Aeronautics and Astronautics, Nanjing 210016, China*

(Received 27 August 2014; published 9 December 2014)

We study a nanosecond electro-optic response of a nematic liquid crystal in a geometry where an applied electric field \mathbf{E} modifies the tensor order parameter but does not change the orientation of the optic axis (director $\hat{\mathbf{N}}$). We use a nematic with negative dielectric anisotropy with the electric field applied perpendicularly to $\hat{\mathbf{N}}$. The field changes the dielectric tensor at optical frequencies (optic tensor) due to the following mechanisms: (a) nanosecond creation of the biaxial orientational order, (b) uniaxial modification of the orientational order that occurs over time scales of tens of nanoseconds, and (c) the quenching of director fluctuations with a wide range of characteristic times up to milliseconds. We develop a model to describe the dynamics of all three mechanisms. We design the experimental conditions to selectively suppress the contributions from the quenching of director fluctuations (c) and from the biaxial order effect (a) and thus, separate the contributions of the three mechanisms in the electro-optic response. As a result, the experimental data can be well fitted with the model parameters. The analysis provides a rather detailed physical picture of how the liquid crystal responds to a strong electric field on a time scale of nanoseconds. The paper provides a useful guidance in the current search for the biaxial nematic phase. Namely, the temperature dependence of the biaxial susceptibility allows one to estimate the temperature of the potential uniaxial-to-biaxial phase transition. An analysis of the quenching of director fluctuations indicates that on a time scale of nanoseconds, the classic model with constant viscoelastic material parameters might reach its limit of validity. The effect of nanosecond electric modification of the order parameter can be used in applications in which one needs to achieve ultrafast (nanosecond) changes in optical characteristics, such as birefringence.

DOI: [10.1103/PhysRevE.90.062504](https://doi.org/10.1103/PhysRevE.90.062504)

PACS number(s): 61.30.Gd, 42.70.Df, 77.84.-s, 78.20.Jq

I. INTRODUCTION

The uniqueness of nematic liquid crystal (NLC) materials is defined by the long-range orientational order of their constituent molecules, which have anisometric shapes and permanent and induced dipoles [1]. The average orientation of NLC molecules in a certain point in space, described by the radius vector \mathbf{r} , is called the director $\hat{\mathbf{N}}(\mathbf{r})$, which coincides with its optic axis. Director orientation can vary from point to point in space or fluctuate in time.

Anisotropic optic and dielectric properties of NLCs, namely, birefringence $\Delta n = n_e - n_o$, where n_e and n_o are the extraordinary and ordinary refractive indices, respectively, and dielectric anisotropy $\Delta\epsilon = \epsilon_{\parallel} - \epsilon_{\perp}$, with ϵ_{\parallel} measured along and ϵ_{\perp} perpendicular to the optic axis, enabled a wide range of electro-optic applications. Traditional electro-optic applications of NLCs are based on the field-induced reorientation of $\hat{\mathbf{N}}$, known as the Frederiks effect. For $\Delta\epsilon > 0$, the director realigns parallel to an applied electric field \mathbf{E} , whereas for $\Delta\epsilon < 0$, it realigns perpendicularly to the field. The characteristic switch-on time is $\tau_{\text{on}}^F = \gamma_1/\epsilon_0|\Delta\epsilon|E^2$, where γ_1 is the rotational viscosity and ϵ_0 is the electric constant. The switch-off time $\tau_{\text{off}}^F = \gamma_1 d^2/K\pi^2$ is typically slower, in the range of milliseconds, being determined by the elastic constant K of the NLC (typically 10 pN) and the cell thickness d (typically 5 μm).

An electro-optic response of the LC, however, can be triggered without director realignment as it suffices to modify the tensorial order parameter (OP) without altering

its orientation [2–12]. An important feature of this approach is that the OP modifications of both uniaxial and biaxial natures take place on the molecular scale and, thus, are very fast (nanoseconds and tens of nanoseconds [12,13]) for both field-on and field-off drivings. For this reason, it is convenient to call the pure OPs-related phenomenon a “nanosecond electric modification of the order parameters” effect or the NEMOPs effect. In addition to the modification of the OPs, the applied field also quenches the director fluctuations [1,11,14–25]. The later effect, being of macroscopic origin, is typically much slower as determined by the length scale of fluctuative director distortions. Both the fundamental understanding and the practical applications of NEMOP require one to separate the fast effects of NEMOP and the slow effects of director fluctuations. This problem and its solution represent one of the main focuses of the presented paper.

In this paper, we demonstrate how to separate the NEMOP effect and the dynamics of director fluctuations by choosing a particular geometry of light propagation through a cell filled with a planar NLC of a negative dielectric anisotropy. The electric field is applied perpendicularly to $\hat{\mathbf{N}}$. Section II presents a theoretical model of the dynamics of the uniaxial and biaxial modifications of the OP and the dynamics of director fluctuations in the electric field. It is shown that the contributions originating in the OP changes and in director fluctuations can be separated from each other by testing the cell under different angles of light incidence. Section III describes the experimental setup to measure the field-induced optic response, which occurs at short time scales down to nanoseconds. Our approach allows one to separate the field-induced birefringence from parasitic effects, such as light scattering. Section IV describes the fitting of the experimental results with the proposed models. Section V discusses the physical

*Current address: Apple, Inc., Cupertino, CA 95014, USA.

†olavrent@kent.edu

mechanisms involved in the ultrafast electro-optic response of an NLC and utilization of the data in evaluating the likelihood of the appearance of a biaxial nematic phase in a field-free state.

II. THEORY

Electro-optic processes could be considered using the free energy functional describing the NLC in the presence of an external electric field,

$$F = \int_V (f_{\text{iso}} + f_m + f_e + f_d) dV \quad (1)$$

where f_{iso} is the free energy density of the isotropic phase for $E = 0$, $f_m = f_m(R_{jk})$ is the phenomenological microscopic free energy density written in the Landau formalism that depends on the scalar OPs R_{jk} , f_e is the elastic free energy density due to distortions of $\hat{\mathbf{N}}$, and $f_d = -\frac{1}{2}\varepsilon_0 \mathbf{E} \boldsymbol{\varepsilon} \mathbf{E}$ is the anisotropic dielectric coupling energy density. The dielectric tensor $\boldsymbol{\varepsilon}$ depends on the OPs R_{jk} and director fluctuations and can be represented as $\boldsymbol{\varepsilon}(R_{jk}, \hat{\mathbf{N}}) = \boldsymbol{\varepsilon}^{(0)}(R_{jk}^{(0)}, \hat{\mathbf{N}}_0) + \delta\boldsymbol{\varepsilon}^{(m)}(R_{jk}, \hat{\mathbf{N}}_0) + \delta\boldsymbol{\varepsilon}^{(f)}(R_{jk}, \hat{\mathbf{N}})$, where $\boldsymbol{\varepsilon}^{(0)}(R_{jk}^{(0)}, \hat{\mathbf{N}}_0)$ is the field-independent tensor defined for a static and uniform (no fluctuations) director $\hat{\mathbf{N}}_0$, $\delta\boldsymbol{\varepsilon}^{(m)}$ is the field-induced modifications associated with the OPs, and $\delta\boldsymbol{\varepsilon}^{(f)}$ is the modification of the tensor caused by the director fluctuations $\delta\hat{\mathbf{N}}(\mathbf{r}) = \hat{\mathbf{N}}(\mathbf{r}) - \hat{\mathbf{N}}_0$, which depend on the applied electric field. We neglect higher-order terms, such as coupling between the director fluctuations and the field-induced changes in OPs. The terms containing $\delta\boldsymbol{\varepsilon}^{(m)}$ in the dielectric energy density f_d define the effect of electrically modified OPs. The term containing $\delta\boldsymbol{\varepsilon}^{(f)}$ in f_d influences the spectrum of director fluctuations.

A. Dynamics of the NEMOP effect

The orientational OPs can be described by the averaged Wigner D functions $\langle D_{jk}^L \rangle$ [26–29] because $D_{jk}^L(\boldsymbol{\Omega})$ forms a complete set of orthogonal functions of the Euler angles $\boldsymbol{\Omega} = \{\omega_1, \omega_2, \omega_3\}$ [30]; $\boldsymbol{\Omega}$ defines the molecular orientation through rotation $\mathbb{L} \xrightarrow{\boldsymbol{\Omega}} \mathbb{M}$ from the laboratory frame \mathbb{L} to the molecular frame \mathbb{M} . A set of OPs $\langle D_{jk}^L \rangle$, obtained by averaging with the single molecule orientational distribution function $f(\boldsymbol{\Omega})$, is complete and equivalent to

$$\langle D_{jk}^L \rangle = \int D_{jk}^L(\boldsymbol{\Omega}) f(\boldsymbol{\Omega}) d\boldsymbol{\Omega}. \quad (2)$$

The nematic phases are described by the OPs with $L = 2$: $R_{jk} = \langle D_{jk}^2 \rangle$. Consider the molecules that possess symmetry C_{2v} or D_{2h} . The Schönflies symbol C_{2v} is assigned to the point group with symmetry operations of identity, rotation around twofold symmetry axis C_2 , and two planes of mirror symmetry containing the C_2 axis. The symbol D_{2h} refers to the point group in which, besides the symmetries above, there are two more C_2 rotation axes, inversion, and the planes of mirror symmetry perpendicular to the C_2 axes. For these molecules, we introduce the molecular frame \mathbb{M} with the axes $\hat{\mathbf{m}}_i$ parallel and perpendicular to the symmetry axis and symmetry plane. The nematic phase formed by these molecules features four independent OPs: two uniaxial OPs, denoted R_{00} , $R_{02} = R_{0-2}$ and two biaxial OPs, denoted $R_{20} = R_{-20}$, $R_{22} = R_{\pm 2\pm 2}$ in

the laboratory frame $\mathbb{L} = Oxyz$ defined by the directors [27–29] with $\hat{\mathbf{N}}_0 = (0, 0, 1)$. The OPs R_{00} and R_{20} describe the uniaxial and biaxial orientational orders, respectively, of the long molecular axes $\hat{\mathbf{m}}_3$ and determine the diagonal form $\{-(R_{00} - \sqrt{6}R_{20})/3, -(R_{00} + \sqrt{6}R_{20})/3, 2R_{00}/3\}$ of the traceless tensor OP $\mathbf{Q} = \langle \hat{\mathbf{m}}_3 \otimes \hat{\mathbf{m}}_3 \rangle - \mathbf{I}/3$ [1,14] in the laboratory frame along the directors. The uniaxial OP R_{00} is nothing else but the standard nematic OP S , $R_{00} = S$. The OPs R_{02} and R_{22} describe the uniaxial and biaxial orderings, respectively, of the short axes $\hat{\mathbf{m}}_{1,2}$ and are equivalent to the tensor $\mathbf{B} = \langle \hat{\mathbf{m}}_1 \otimes \hat{\mathbf{m}}_1 - \hat{\mathbf{m}}_2 \otimes \hat{\mathbf{m}}_2 \rangle$ [31], which has the diagonal form $\{-(\sqrt{2}R_{02} - 2\sqrt{3}R_{22})/3, -(\sqrt{2}R_{02} + 2\sqrt{3}R_{22})/3, 2\sqrt{2}R_{02}/3\}$ in the laboratory frame along the directors. Without the electric field, the NLC under consideration is uniaxial with the equilibrium uniaxial OPs $R_{00}^{(0)}$ and $R_{02}^{(0)}$, whereas the biaxial OPs are zero, $R_{20}^{(0)} = R_{22}^{(0)} = 0$. The electric field \mathbf{E} changes the OPs $\delta R_{jk} = R_{jk} - R_{jk}^{(0)}$ through $\delta\boldsymbol{\varepsilon}^{(m)}$. When δR_{jk} is small and the field is applied along one of the laboratory axes, the diagonal elements $\{\delta\varepsilon_x, \delta\varepsilon_y, \delta\varepsilon_z\}$ of the dielectric tensor $\delta\boldsymbol{\varepsilon}^{(m)}$ are

$$\delta\varepsilon_i = \sum_{j,k=0,2} \varepsilon_{i,jk} \delta R_{jk}, \quad i = x, y, z, \quad (3)$$

where $\varepsilon_{i,jk} = \partial\varepsilon_i / \partial(\delta R_{jk})_{\boldsymbol{\varepsilon}=\boldsymbol{\varepsilon}^{(0)}}$. Rotation of \mathbb{L} by $\pi/2$ around Oz changes the sign of the biaxial OPs δR_{2k} but does not affect the uniaxial OPs δR_{0k} . This results in the following properties: (a) $\varepsilon_{z,2k} = 0$ and, therefore, $\delta\varepsilon_z$ contains only the uniaxial OPs δR_{0k} , (b) the relation $\varepsilon_{y,jk} = (-1)^{j/2} \varepsilon_{x,jk}$ stands, and (c) the quadratic expansion of microscopic f_m near the zero-field equilibrium value $f_m^{(0)}$ with $R_{jk} = R_{jk}^{(0)}$ does not contain cross terms of the uniaxial and biaxial OPs:

$$f_m = f_m^{(0)} + \frac{1}{2} \sum_{j,k,k'} M_{jk,jk'} \delta R_{jk} \delta R_{jk'}, \quad (4)$$

where $M_{jk,jk'} = (\partial^2 f_m / \partial R_{jk} \partial R_{jk'})_{R_{jk}=R_{jk}^{(0)}}$ are the Taylor coefficients that can be determined from the Landau expansion of the free energy for uniaxial and biaxial nematics [32] and indices j, k , and k' run through two values 0 and 2. Because we consider processes with characteristic times less than a microsecond, the heat transfer is negligible [33], and therefore, $M_{jk,jk'}$ corresponds to the expansion under adiabatic conditions.

We model the dynamics of the four OPs, $\delta R_{jk} = \delta R_{00}$, δR_{02} , δR_{20} , and δR_{22} using the standard Landau-Khalatnikov approach [34],

$$\begin{aligned} \gamma_{jk} \frac{d(\delta R_{jk})}{dt} &= -\frac{\partial(f_d + f_m)}{\partial(\delta R_{jk})} \\ &= G_{jk} E^2(t) - \sum_{k'} M_{jk,jk'} \delta R_{jk'}, \end{aligned} \quad (5)$$

where $G_{jk} = \frac{\varepsilon_0}{2} \sum_i \varepsilon_{i,jk} e_i^2$, e_i are the components of the unit vector $\hat{\mathbf{e}}$ directed along the applied electric field $\mathbf{E}(t)$, and γ_{jk} is the rotational viscosity for the OP δR_{jk} . We neglect the effects of the director reorientation and associated flows on the OPs, discussed in Refs. [35,36], because we consider the geometries when the applied electric field stabilizes the director $\hat{\mathbf{N}}_0$. Four Eqs. (5) are two independent pairs of linear inhomogeneous

ordinary differential equations with constant coefficients for the uniaxial δR_{0k} and biaxial δR_{2k} OPs and could be written in a vector form

$$\xi_{(j)} \frac{d}{dt} \mathbf{R}^{(j)} = \xi_{(j)}^{-1} \mathbf{G}^{(j)} E^2(t) - \bar{\mathbf{M}}^{(j)} \xi_{(j)} \mathbf{R}^{(j)}, \quad (6)$$

where $\mathbf{R}^{(j)} = \begin{pmatrix} \delta R_{j0} \\ \delta R_{j2} \end{pmatrix}$, $\mathbf{G}^{(j)} = \begin{pmatrix} G_{j0} \\ G_{j2} \end{pmatrix}$, $\xi_{(j)} = \begin{pmatrix} \gamma_{j0}^{1/2} & 0 \\ 0 & \gamma_{j2}^{1/2} \end{pmatrix}$, and $\bar{\mathbf{M}}^{(j)}$ is the 2×2 symmetric matrix with elements $\bar{M}_{kk'}^{(j)} = \gamma_{jk}^{-1/2} M_{jk,jk'} \gamma_{jk'}^{-1/2}$. The solution for Eq. (6) $\mathbf{R}^{(j)}(t)$ can be expressed through the vector of decoupled relaxation modes $\mathbf{r}^{(j)}(t) = \begin{pmatrix} r_{0,2}^{(j)}(t) \\ r_{2,2}^{(j)}(t) \end{pmatrix}$,

$$\mathbf{R}^{(j)}(t) = \xi_{(j)}^{-1} \mathbf{V}^{(j)} \mathbf{r}^{(j)}(t), \quad (7)$$

where $\mathbf{V}^{(j)}$ is the matrix of eigenvectors of $\bar{\mathbf{M}}^{(j)}$ that obeys the equation $\bar{\mathbf{M}}^{(j)} \mathbf{V}^{(j)} = \mathbf{V}^{(j)} \mathbf{\Lambda}^{(j)}$; here $\mathbf{\Lambda}^{(j)} = \begin{pmatrix} \lambda_{0,2}^{(j)} & 0 \\ 0 & \lambda_{2,2}^{(j)} \end{pmatrix}$ is a diagonal matrix of the eigenvalues $\lambda_{0,2}^{(j)}$. Since $\bar{\mathbf{M}}^{(j)}$ is a symmetric positively defined matrix, $\mathbf{V}^{(j)} = \begin{pmatrix} \cos \phi_j & -\sin \phi_j \\ \sin \phi_j & \cos \phi_j \end{pmatrix}$ is an orthogonal matrix and is determined by the eigenvector angle ϕ_j , which satisfies the equation,

$$\tan 2\phi_j = 2\bar{M}_{02}^{(j)} / (\bar{M}_{00}^{(j)} - \bar{M}_{22}^{(j)}). \quad (8)$$

It is also convenient to use ϕ_j in the expression for $\lambda_{0,2}^{(j)} = \frac{1}{2} [\bar{M}_{00}^{(j)} + \bar{M}_{22}^{(j)} \pm (\bar{M}_{00}^{(j)} - \bar{M}_{22}^{(j)}) / \cos 2\phi_j]$ because selection $|\phi_j| < \pi/4$ as the range of solutions of Eq. (8) ensures that the dynamics of the uniaxial OPs δR_{jk} are mainly controlled by $r_k^{(j)}(t)$ with the corresponding relaxation time $\tau_k^{(j)} = 1/\lambda_k^{(j)}$,

$$r_k^{(j)}(t) = g_k^{(j)} \int_0^t E^2(t') \exp[(t' - t)/\tau_k^{(j)}] dt', \quad (9)$$

where $g_k^{(j)}$ are the components of the vector $\mathbf{g}^{(j)} = (\mathbf{V}^{(j)})^{-1} \xi_{(j)}^{-1} \mathbf{G}^{(j)}$.

To describe the optic manifestation of the NEMOP effect, we use the OPs-related deviation $\delta \tilde{\epsilon}^{(m)}$ of the dielectric tensor at optical frequency (optic tensor) from its zero-field value $\tilde{\epsilon}^{(0)}$. Here and in what follows, tildes represent a reference to the material parameters at the optical frequencies. In the laboratory frame $Oxyz$ along the directors, the tensor $\delta \tilde{\epsilon}^{(m)}$ has the diagonal form $\{\delta \tilde{\epsilon}_x, \delta \tilde{\epsilon}_y, \delta \tilde{\epsilon}_z\}$ and can be split into an isotropic $\delta \tilde{\epsilon}_{\text{iso}}$, uniaxial $\delta \tilde{\epsilon}_u$, and biaxial $\delta \tilde{\epsilon}_b$ contributions,

$$\begin{aligned} \delta \tilde{\epsilon}_x &= \delta \tilde{\epsilon}_{\text{iso}} - \frac{1}{3} \delta \tilde{\epsilon}_u + \frac{1}{2} \delta \tilde{\epsilon}_b, \\ \delta \tilde{\epsilon}_y &= \delta \tilde{\epsilon}_{\text{iso}} - \frac{1}{3} \delta \tilde{\epsilon}_u - \frac{1}{2} \delta \tilde{\epsilon}_b, \\ \delta \tilde{\epsilon}_z &= \delta \tilde{\epsilon}_{\text{iso}} + \frac{2}{3} \delta \tilde{\epsilon}_u. \end{aligned} \quad (10)$$

Since $\delta \epsilon^{(m)}$ and $\delta \tilde{\epsilon}^{(m)}$ are the same tensor at different frequencies, the deviations $\delta \tilde{\epsilon}_i = \sum_{j,k=0,2} \tilde{\epsilon}_{i,jk} \delta R_{jk}$ should be also linear in δR_{jk} , where $\tilde{\epsilon}_{i,jk} = \partial \tilde{\epsilon}_i / \partial (\delta R_{jk})_{\tilde{\epsilon}=\tilde{\epsilon}^{(0)}}$ have the same symmetry properties as $\epsilon_{i,jk}$. Then, the dynamics of $\delta \tilde{\epsilon}_{\text{iso}}$ and $\delta \tilde{\epsilon}_u$ are controlled by the uniaxial OPs δR_{0k} and therefore, by the vector of uniaxial modes $\mathbf{r}^{(0)}(t)$, whereas $\delta \tilde{\epsilon}_b$ is controlled by the biaxial OPs δR_{2k} and by $\mathbf{r}^{(2)}(t)$,

$$\begin{aligned} \delta \tilde{\epsilon}_{\text{iso}}(t) &= \tilde{\mathbf{h}}^{(\text{iso})} \xi_{(0)}^{-1} \mathbf{V}^{(0)} \mathbf{r}^{(0)}(t), \\ \delta \tilde{\epsilon}_u(t) &= \tilde{\mathbf{h}}^{(u)} \xi_{(0)}^{-1} \mathbf{V}^{(0)} \mathbf{r}^{(0)}(t), \\ \delta \tilde{\epsilon}_b(t) &= \tilde{\mathbf{h}}^{(b)} \xi_{(2)}^{-1} \mathbf{V}^{(2)} \mathbf{r}^{(2)}(t), \end{aligned} \quad (11)$$

where $\tilde{\mathbf{h}}^{(\text{iso})}$, $\tilde{\mathbf{h}}^{(u)}$, and $\tilde{\mathbf{h}}^{(b)}$, respectively, are vectors with components $\tilde{h}_k^{(\text{iso})} = \frac{1}{3}(\tilde{\epsilon}_{x,0k} + \tilde{\epsilon}_{y,0k} + \tilde{\epsilon}_{z,0k})$, $\tilde{h}_k^{(u)} = \tilde{\epsilon}_{z,0k} - (\tilde{\epsilon}_{x,0k} + \tilde{\epsilon}_{y,0k})/2$, and $\tilde{h}_k^{(b)} = \tilde{\epsilon}_{x,2k} - \tilde{\epsilon}_{y,2k}$.

The dynamics of the NEMOP effect is described by two uniaxial and two biaxial relaxation modes, Eqs. (9) and (11). When \mathbf{E} is perpendicular to the Oz axis (chosen parallel to the director) and $\Delta \epsilon < 0$, all four modes should contribute to the optic response. However, as we will show below our experimental data for dielectrically negative material 4'-butyl-4-heptyl-bicyclohexyl-4-carbonitrile (CCN-47) are fitted well by the simplified version of the model with one uniaxial mode and one biaxial mode. We explain this fact with the assumption that the NEMOP effect is controlled by the following two modes: (i) $r_0^{(0)}(t)$, associated mainly with the uniaxial OP $R_{00} = S$ of the long molecular axes, and (ii) $r_2^{(2)}(t)$, associated mainly with the biaxial OP R_{22} of the short molecular axes. These two OPs are predicted to be dominant in the spontaneous (field-free) uniaxial and biaxial NLC [32,37]. The same OPs are expected to play a major role in the NEMOP experiments since δR_{00} causes strong changes in optic anisotropy (large $\tilde{h}_0^{(u)}$) and δR_{22} is strongly affected by the interactions between the transverse molecular dipoles and the electric field (large G_{22}). In this two-mode assumption, the isotropic $\delta \tilde{\epsilon}_{\text{iso}}$, uniaxial $\delta \tilde{\epsilon}_u$, and biaxial $\delta \tilde{\epsilon}_b$ contributions Eq. (11) are simplified

$$\delta \tilde{\epsilon}_{\bar{j}}(t) = \frac{\alpha_{\bar{j}}}{\tau_{\bar{j}}} \int_0^t E^2(t') \exp[(t' - t)/\tau_{\bar{j}}] dt', \quad (12)$$

where \bar{j} reads iso, u , or b depending on the nature of contribution, $\tau_u = \tau_{\text{iso}} = \tau_0^{(u)} \approx \gamma_{00}/M_{00,00}$ and $\tau_b = \tau_2^{(b)} \approx \gamma_{22}/M_{22,22}$ are the uniaxial and biaxial relaxation times, and $\alpha_u \approx \tilde{h}_0^{(u)} G_{00}/M_{00,00}$ and $\alpha_b \approx \tilde{h}_2^{(b)} G_{22}/M_{22,22}$ are the effective uniaxial and biaxial susceptibilities, respectively. One can expect that τ_u , determined by reorientation of the long axes, is substantially larger than τ_b , determined by rotation of the short axes because the former process is associated with the larger moment of inertia and requires stronger readjustment of the neighboring molecules. For the electric field parallel to the Ox axis $\hat{\mathbf{e}} = (1, 0, 0)$, one can estimate

$$\begin{aligned} \alpha_u &\approx \epsilon_0 \epsilon_{x,00} \tilde{\epsilon}_{x,00} / 2M_{00,00}, \\ \alpha_b &\approx \epsilon_0 \epsilon_{x,22} \tilde{\epsilon}_{x,22} / M_{22,22}. \end{aligned} \quad (13)$$

The uniaxial $\delta \tilde{\epsilon}_u$ and biaxial $\delta \tilde{\epsilon}_b$ terms provide the main contributions to the NEMOP. The dynamics of the isotropic term $\delta \tilde{\epsilon}_{\text{iso}}$ is similar to that of $\delta \tilde{\epsilon}_u$, but its contribution is relatively small: $\delta \tilde{\epsilon}_{\text{iso}} = 0$ under the assumption that $\tilde{\epsilon}$ is an orientational average of the molecular polarizability tensor because $\text{Tr } \tilde{\epsilon} = \sum_i \tilde{\epsilon}_i = \text{const}$ in this case [32], and the only nonzero contribution to $\delta \tilde{\epsilon}_{\text{iso}}$ stems from the dipole-dipole resonance and dispersion intermolecular interactions [38]. Moreover, $\delta \tilde{\epsilon}_{\text{iso}}$ does not contribute to the response caused by changes in birefringence.

B. Dynamics of director fluctuations in the electric field

Besides the NEMOP effect, the electric field provides an additional electro-optic response, which is of macroscopic nature. In NLCs with a negative dielectric anisotropy, the electric field $\mathbf{E} = (E, 0, 0)$ does not reorient the average

$\hat{\mathbf{N}}_0 = (0,0,1)$ but modifies the director fluctuations $\delta\mathbf{N} = \hat{\mathbf{N}} - \hat{\mathbf{N}}_0$. We analyze this effect using the macroscopic part of free energy $\bar{F} = \int_V (f_e + \bar{f}_d) dV$, where $V = d \times L_y \times L_z$ is the active volume of the cell, covered by the electrodes of the area $L_y \times L_z$ and d is the thickness of the NLC layer. The elastic energy density f_e is

$$f_e = \frac{1}{2} [K_1 (\text{div } \hat{\mathbf{N}})^2 + K_2 (\hat{\mathbf{N}} \cdot \text{curl } \hat{\mathbf{N}})^2 + K_3 (\hat{\mathbf{N}} \times \text{curl } \hat{\mathbf{N}})^2], \quad (14)$$

where K_1 , K_2 , and K_3 are the Frank elasticity constants for splay, twist, and bend, respectively. The dielectric energy density associated with the director distortions $\bar{f}_d = -\frac{1}{2} \varepsilon_0 \mathbf{E} \bar{\boldsymbol{\varepsilon}} \mathbf{E}$ is determined by the corresponding part of the dielectric tensor $\bar{\boldsymbol{\varepsilon}} = \boldsymbol{\varepsilon}^{(0)}(R_{jk}^{(0)}, \hat{\mathbf{N}}_0) + \delta \boldsymbol{\varepsilon}^{(fl)}(R_{jk}^{(0)}, \hat{\mathbf{N}}) = \varepsilon_{\perp}^{(0)} \mathbf{I} + (\varepsilon_{\parallel}^{(0)} - \varepsilon_{\perp}^{(0)}) \hat{\mathbf{N}} \otimes \hat{\mathbf{N}}$, where \mathbf{I} is the unit tensor, $\varepsilon_{\perp}^{(0)}$ and $\varepsilon_{\parallel}^{(0)}$ are the dielectric constants, perpendicular and parallel to $\hat{\mathbf{N}}_0$, and \otimes denotes the outer product.

We assume that the director fluctuations $\delta\mathbf{N} = [N_x(\mathbf{r}), N_y(\mathbf{r}), 0]$ are small, periodic in the Oyz area of V , and obey the strong anchoring boundary conditions at the substrates. Thus we expand $\delta\mathbf{N}$ in Fourier series, similar to [39]

$$\delta\mathbf{N}(\mathbf{r}) = \sum_{\mathbf{q}} \mathbf{N}(\mathbf{q}) \sin(q_x x) \exp[i(q_y y + q_z z)], \quad (15)$$

where $\mathbf{q} = (q_x, q_y, q_z) = (\frac{\pi}{d} k, \frac{2\pi}{L_y} l, \frac{2\pi}{L_z} m)$ are discrete wave vectors with $k > 0$, l , and m being integers.

Using Eq. (15) and integrating over V , we obtain \bar{F} associated with the director fluctuations in the Gaussian approximation,

$$\begin{aligned} \bar{F} = & \frac{V}{4} \sum_{\mathbf{q}} [(K_1 q_x^2 + K_2 q_y^2 + K_3 q_z^2 - \varepsilon_0 \Delta \varepsilon^{(0)} E_x^2) |N_x^2(\mathbf{q})| \\ & + (K_1 q_y^2 + K_2 q_x^2 + K_3 q_z^2) |N_y^2(\mathbf{q})|] + 2\pi i L_z (K_1 - K_2) \\ & \times \sum_{\mathbf{q}, \mathbf{q}'} [N_x(\mathbf{q}) N_y^*(\mathbf{q}') + N_x^*(\mathbf{q}') N_y(\mathbf{q})] \frac{klk'}{(k^2 - k'^2)}, \quad (16) \end{aligned}$$

where the latter sum contains the cross terms of $N_x(\mathbf{q})$ and $N_y(\mathbf{q}')$ with $(k - k')$ being an odd number, $l = l'$, and $m = m'$.

To describe the dynamics of fluctuations, we start with the Langevin equation by including the random force $\zeta_{\alpha}(t, \mathbf{q})$ in the viscous relaxation equation for $N_{\alpha}(t, \mathbf{q})$, $\alpha = x, y$ [1, 16, 25] and use the splay-twist one-constant approximation $K_1 = K_2 = \bar{K}$, which diagonalizes the free energy Eq. (16) with respect to $N_x(\mathbf{q})$ and $N_y(\mathbf{q})$,

$$\eta_{\alpha}(\hat{\mathbf{q}}) \frac{dN_{\alpha}(t, \mathbf{q})}{dt} = -f_{\alpha}(t, \mathbf{q}) N_{\alpha}(t, \mathbf{q}) + \zeta_{\alpha}(t, \mathbf{q}), \quad (17)$$

where $f_y(t, \mathbf{q}) = f_K(\mathbf{q}) = \bar{K}(q_x^2 + q_y^2) + K_3 q_z^2$, $f_x(t) = f_K(\mathbf{q}) + f_E(t, \mathbf{q})$, $f_E(t) = \varepsilon_0 |\Delta \varepsilon| E^2(t)$, and $\eta_{\alpha}(\hat{\mathbf{q}}) = \gamma_1 - \Delta \eta_{\alpha}(\hat{\mathbf{q}})$ is the effective director viscosity; here γ_1 is the director rotational viscosity and $\Delta \eta_{\alpha}(\hat{\mathbf{q}})$ is the backflow effect's correction, which, in the hydrodynamic limit of small \mathbf{q} , depends on $\hat{\mathbf{q}} = \mathbf{q}/|\mathbf{q}|$ [1, 16, 25]. The random force $\zeta_{\alpha}(t, \mathbf{q})$ has the standard

“white noise” properties with the noise strength $Z_{\alpha}(t, \mathbf{q})$,

$$\begin{aligned} \langle \zeta_{\alpha}(t, \mathbf{q}) \rangle &= 0, \\ \langle \zeta_{\alpha}(t, \mathbf{q}) \zeta_{\alpha'}^*(t', \mathbf{q}') \rangle &= Z_{\alpha}(t, \mathbf{q}) \delta(t - t') \delta_{\mathbf{q}\mathbf{q}'} \delta_{\alpha\alpha'}, \quad (18) \end{aligned}$$

where the brackets $\langle \dots \rangle$ denote an ensemble average. The solution of Eq. (17),

$$N_{\alpha}(t, \mathbf{q}) = e^{-S_{\alpha}(t, \mathbf{q})} \left[N_{\alpha}(0, \mathbf{q}) + \eta_{\alpha}^{-1}(\hat{\mathbf{q}}) \int_0^t e^{S_{\alpha}(t', \mathbf{q})} \zeta_{\alpha}(t', \mathbf{q}) dt' \right], \quad (19)$$

where $S_{\alpha}(t, \mathbf{q}) = \eta_{\alpha}^{-1} \int_0^t f_{\alpha}(t', \mathbf{q}) dt'$ allows us to derive the equation that controls the dynamics of ensemble averaged fluctuations $\langle |N_{\alpha}^2(t, \mathbf{q})| \rangle$,

$$\tau_{\alpha}(t, \mathbf{q}) \frac{d \langle |N_{\alpha}^2(t, \mathbf{q})| \rangle}{dt} = \frac{Z_{\alpha}(t, \mathbf{q})}{2\eta_{\alpha}(\hat{\mathbf{q}}) f_{\alpha}(t, \mathbf{q})} - \langle |N_{\alpha}^2(t, \mathbf{q})| \rangle, \quad (20)$$

where $\tau_{\alpha}(t, \mathbf{q}) = \eta_{\alpha}(\hat{\mathbf{q}})/2f_{\alpha}(t, \mathbf{q})$ is the characteristic relaxation time. For the stationary electric field E , the averaged fluctuations $\langle |N_{\alpha}^2(t, \mathbf{q})| \rangle$ can be calculated using the equipartition theorem and the free energy Eq. (16), $\langle |N_{\alpha}^2(t, \mathbf{q})| \rangle_E = \frac{2k_B T}{V f_{\alpha}(t, \mathbf{q})}$, thus $Z_{\alpha}(t, \mathbf{q}) = \frac{2k_B T}{V} \eta_{\alpha}(\hat{\mathbf{q}})$.

The fluctuations along the y axis are not affected by the applied field $\langle |N_y^2(t, \mathbf{q})| \rangle = \langle |N_y^2(0, \mathbf{q})| \rangle$, and only the dynamics of $\langle |N_x^2(t, \mathbf{q})| \rangle$ affects the optic response. Introducing the field-induced quenching of fluctuations $\mathfrak{N}(t, \mathbf{q}) = \langle |N_x^2(t, \mathbf{q})| \rangle - \langle |N_x^2(0, \mathbf{q})| \rangle$, which satisfies the initial condition $\mathfrak{N}(0, \mathbf{q}) = 0$, we obtain the solution of Eq. (20) as

$$\mathfrak{N}(t, \mathbf{q}) = \frac{4k_B T}{V \eta_x(\hat{\mathbf{q}}) f_K(\mathbf{q})} \int_0^t f_E(t') \exp \left[- \int_{t'}^t \frac{dt''}{\tau_x(\mathbf{q})} \right] dt'. \quad (21)$$

For a strong applied field, the electro-optic response is caused by the quenching of director fluctuations with a broad range of \mathbf{q} . Thus, we neglect the hydrodynamic effects and use an approximation of the constant effective rotational viscosity γ_{eff} for the director fluctuations in the entire range of \mathbf{q} . In this case the solution Eq. (21) is simplified to

$$\begin{aligned} \mathfrak{N}(t, \mathbf{q}) = & \frac{2k_B T}{V \gamma_{\text{eff}} f_K(\mathbf{q})} e^{-S(t)} \int_0^t f_E(t') \\ & \times \exp \left[- \frac{f_K(\mathbf{q})(t - t')}{\gamma_{\text{eff}}} \right] e^{S(t')} dt', \quad (22) \end{aligned}$$

where $S(t) = \frac{1}{\gamma_{\text{eff}}} \int_0^t f_E(t') dt'$ and $\gamma_{\text{eff}} \approx \gamma_1/2$.

Because the electric field affects only the director fluctuations along the x axis $\langle N_x^2(t, \mathbf{r}) \rangle$, the associated modifications of the optic tensor are

$$\begin{aligned} \delta \bar{\varepsilon}_z^{(fl)}(t, \mathbf{r}) &= -\delta \bar{\varepsilon}_x^{(fl)}(t, \mathbf{r}) \\ &= -(\langle N_x^2(t, \mathbf{r}) \rangle - \langle N_x^2(0, \mathbf{r}) \rangle) (n_e^2 - n_o^2), \quad (23) \end{aligned}$$

where n_o and n_e are the ordinary and extraordinary refractive indices, respectively, measured in the field-free state $E = 0$.

In our experiments, we use a probing laser beam of half millimeter diameter and measure the phase retardation which is an integral along the cell thickness; thus, the fluctuations' contribution is determined by Eq. (23) averaged over the active

volume of the cell,

$$\delta\tilde{\varepsilon}_f(t) = V^{-1} \int_V \delta\tilde{\varepsilon}_z^{(f)}(t, \mathbf{r}) d\mathbf{r} = \frac{(n_e^2 - n_o^2)}{2} \sum_{\mathbf{q}} \mathfrak{N}(t, \mathbf{q}). \quad (24)$$

The applied electric field affects the fluctuations for which $q < q_c = \sqrt{\Delta\varepsilon \varepsilon_0 E^2 / \bar{K}}$ as follows from the inequality $f_K(\mathbf{q}) < f_E$. For the strong electric field ($E \sim 10^8$ V/m), the number of these fluctuations is very large as the maximum values of the integer indices are as follows: $k_{\max} > 10^3$ and $l_{\max}, m_{\max} > 10^5$. Thus, we neglect the discrete nature of \mathbf{q} and transform the sum Eq. (24) into an integral where we stretch $q_z, \mathbf{q} \rightarrow \bar{\mathbf{q}} = (q_x, q_y, \sqrt{K_3/\bar{K}}q_z)$. This transformation makes the elastic term $f_K(\bar{\mathbf{q}}) = \bar{K} \bar{q}^2$ isotropic and, therefore, $\mathfrak{N}(t, \bar{\mathbf{q}})$ also becomes isotropic,

$$\delta\tilde{\varepsilon}_f(t) = (n_e^2 - n_o^2) \frac{V\sqrt{\bar{K}}}{8\pi^3\sqrt{K_3}} \int_{V_{\bar{\mathbf{q}}}} \mathfrak{N}(t, \bar{\mathbf{q}}) d\bar{\mathbf{q}}, \quad (25)$$

where the integration volume $V_{\bar{\mathbf{q}}}$ is defined by conditions $\bar{q}_x \geq \pi/d$ and $\bar{q} < q_c = \pi/a_c$. Here the first condition stems from the strong anchoring at the substrates, and a_c is the characteristic distance that corresponds to the breakdown of continuum theory. Integrating (25) using (22), we obtain the contribution of the field-quenched director fluctuations for modification of the optic tensor,

$$\delta\tilde{\varepsilon}_f(t) = A \frac{e^{-S(t)}}{\sqrt{\gamma_{\text{eff}}}} \int_0^t \frac{f_E(t')e^{S(t')}}{\sqrt{t-t'}} \left\{ \text{erf} \sqrt{\frac{t-t'}{\tau_c}} - \text{erf} \sqrt{\frac{t-t'}{\tau_d}} - \sqrt{\frac{t-t'}{\pi\tau_d}} \left[E_1\left(\frac{t-t'}{\tau_d}\right) - E_1\left(\frac{t-t'}{\tau_c}\right) \right] \right\} dt', \quad (26)$$

$$\delta n_{\text{eff}} = \frac{\delta\tilde{\varepsilon}_x \tilde{k}_{xe} (\tilde{k}_z^2 \tilde{k}_{xe} \tilde{k}_{xo} - \tilde{k}_y^2 n_o^2) + \delta\tilde{\varepsilon}_y (\tilde{k}_y^2 \tilde{k}_z^2 \tilde{k}_{xo} - \tilde{k}_{xe} n_o^2 \tilde{k}_{xo}^2) + \delta\tilde{\varepsilon}_z (n_o^2 - \tilde{k}_z^2) \tilde{k}_{xo}}{2\tilde{k}_{xe} \tilde{k}_{xo} n_o^2 (n_o^2 - \tilde{k}_z^2)}. \quad (28)$$

The optic tensor modifications $\delta\tilde{\varepsilon}_x$, $\delta\tilde{\varepsilon}_y$, and $\delta\tilde{\varepsilon}_z$ contain the uniaxial $\delta\tilde{\varepsilon}_u$ and isotropic $\delta\tilde{\varepsilon}_{\text{iso}}$ contributions associated with the field-enhanced uniaxial order, the term stemmed from the field-induced biaxial order $\delta\tilde{\varepsilon}_b$, and the contribution $\delta\tilde{\varepsilon}_f$ caused by the quenching of director fluctuations along the x axis. In real samples, there is also an additional ‘‘pretilt’’ term because the surface alignment direction at the bounding plates is practically never strictly parallel to the plate due to the small pretilt angle β induced by rubbing of the aligning layer. Nonzero β implies that the zero-field director and the field are not strictly orthogonal and that there is a nonzero dielectric torque on the director. The corresponding change in the effective birefringence is proportional to $(\bar{\beta} - \bar{\beta}_0)$, where $\bar{\beta}$ and $\bar{\beta}_0$ are the averaged angles between the director and the substrate plane with and without the applied electric field, respectively. One can show that $\bar{\beta}_0$ is the arithmetic mean of the pretilt angles at the top and bottom plates.

Using Eqs. (10) and (23) for the discussed contributions, we obtain from Eq. (28),

$$\delta n_{\text{eff}} = \sigma_{bu} (\delta\tilde{\varepsilon}_u + \frac{3}{2} \delta\tilde{\varepsilon}_b) + \sigma_{uf} (\delta\tilde{\varepsilon}_u + \frac{3}{2} \delta\tilde{\varepsilon}_f) + \sigma_{\beta} (\bar{\beta} - \bar{\beta}_0), \quad (29)$$

where $A = (n_e^2 - n_o^2) \frac{k_B T}{2\pi^{3/2} \bar{K} \sqrt{K_3}}$, $\tau_d = \frac{\gamma_{\text{eff}} d^2}{K \pi^2} \approx \tau_{\text{off}}^F / 2$, $\tau_c = \frac{\gamma_{\text{eff}}}{K_3 q_c^2}$, and $E_1(t) = \int_t^\infty \frac{e^{-t'}}{t'} dt'$ ($t > 0$) is the exponential integral, see, e.g., Chap. 5 of Ref. [40].

C. Analysis and optimization of experimental geometries

We describe optical properties using the normalized wave vectors $\tilde{\mathbf{k}} = \frac{\lambda}{2\pi} \mathbf{k}$ of the optical modes, where λ is the wavelength of a probing beam in vacuum. The tangential components \tilde{k}_y and \tilde{k}_z are preserved at interfaces between different layers: glass, indium tin oxide (ITO), polymer, nematic, etc., and are the same for all optical modes. The optical retardance between the two forward modes propagating through the field-induced (effectively biaxial) states of an NLC $\Gamma = \Delta n_{\text{eff}} d$ is determined by the NLC thickness d and the effective birefringence $\Delta n_{\text{eff}} = \tilde{k}_x^{(1)} - \tilde{k}_x^{(2)}$, where $\tilde{k}_x^{(1)}$ and $\tilde{k}_x^{(2)}$ are solutions of the Fresnel equation for two forward propagating modes $\tilde{k}_x > 0$ in the biaxial medium,

$$\tilde{\varepsilon}_x \tilde{k}_x^4 - Q_2 \tilde{k}_x^2 + Q_0 = 0, \quad (27)$$

where $Q_2 = \tilde{\varepsilon}_x (\tilde{\varepsilon}_y + \tilde{\varepsilon}_z) - \tilde{k}_y^2 (\tilde{\varepsilon}_x + \tilde{\varepsilon}_y) - \tilde{k}_z^2 (\tilde{\varepsilon}_x + \tilde{\varepsilon}_z)$ and $Q_0 = (\tilde{\varepsilon}_y \tilde{\varepsilon}_z - \tilde{\varepsilon}_y \tilde{k}_y^2 - \tilde{\varepsilon}_z \tilde{k}_z^2) (\tilde{\varepsilon}_x - \tilde{k}_y^2 - \tilde{k}_z^2)$. In the field-free uniaxial state, modes 1 and 2 are the extraordinary $\tilde{k}_x^{(1)} = k_{xe} = \sqrt{n_e^2 (1 - \frac{\tilde{k}_z^2}{n_o^2}) - \tilde{k}_y^2}$ and ordinary $\tilde{k}_x^{(2)} = k_{xo} = \sqrt{n_o^2 - \tilde{k}_y^2 - \tilde{k}_z^2}$ waves, respectively. An applied electric field causes a change in the effective birefringence $\delta n_{\text{eff}} = (\tilde{k}_x^{(1)} - k_{xe}) - (\tilde{k}_x^{(2)} - k_{xo})$, calculated from Eq. (27),

where $\sigma_{bu} = \frac{1}{6n_o^2(n_o^2 - \tilde{k}_z^2)} [\tilde{k}_z^2 (\tilde{k}_{xe} - \frac{\tilde{k}_y^2}{\tilde{k}_{xe}}) + n_o^2 (\tilde{k}_{xo} - \frac{\tilde{k}_y^2}{\tilde{k}_{xo}})]$, $\sigma_{uf} = \frac{1}{3n_o^2} [\frac{n_o^2 - \tilde{k}_z^2}{\tilde{k}_{xe}} + \frac{\tilde{k}_y^2 n_o^2 - \tilde{k}_z^2 \tilde{k}_{xo} \tilde{k}_{xe}}{\tilde{k}_{xo} (n_o^2 - \tilde{k}_z^2)}]$, and $\sigma_{\beta} = \frac{n_e^2 - n_o^2}{n_o^2} \tilde{k}_z$ are the weighting coefficients dependent on an experimental geometry. Note that $\delta\tilde{\varepsilon}_{\text{iso}}$ does not contribute to δn_{eff} and therefore cannot be extracted from the phase retardance measurements. We also cannot completely separate $\delta\tilde{\varepsilon}_u$, $\delta\tilde{\varepsilon}_b$, and $\delta\tilde{\varepsilon}_f$ by staging three different experimental geometries because these terms appear in Eq. (29) in two combinations. However, as we will show below, there is a possibility to determine $\delta\tilde{\varepsilon}_u$, $\delta\tilde{\varepsilon}_b$, and $\delta\tilde{\varepsilon}_f$ independently utilizing their distinct dynamics.

We perform experiments for the following three geometries that provide the simplest interpretation:

(a) ‘‘Biaxial-uniaxial’’ (BU) geometry in which the contribution of director fluctuations is eliminated, $\sigma_{uf} = 0$, and only the biaxial and uniaxial OPs contribute to the optic response.

(b) ‘‘Uniaxial-fluctuations’’ (UF) geometry: Only the uniaxial OPs and director fluctuations contribute to the optic response, whereas the biaxial contribution does not, $\sigma_{bu} = 0$.

(c) ‘‘Normal’’ (N) geometry with the perpendicular incidence of a probing beam in which case all the three

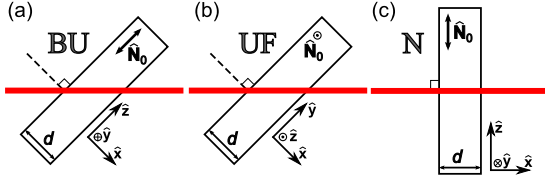


FIG. 1. (Color online) Three experimental schemes for testing an electro-optic response of a nematic cell with the laser beam (horizontal red line). (a) BU geometry probing biaxial and uniaxial contributions to the optic response. (b) UF geometry probing uniaxial and fluctuations quenching modifications. (c) N geometry, all three mechanisms contribute to the optic response.

mechanisms (uniaxial, biaxial, and fluctuation quenchings) contribute to the measured signal, but the experimental setting and weighting coefficients in Eq. (29) are simple.

1. Biaxial-uniaxial geometry

The simplest of the BU geometries, that satisfies the condition $\sigma_{uf} = 0$, is the one in which the incidence plane of a probing beam contains the director $\tilde{k}_y = 0$, and the incidence angle obeys the condition $\tilde{k}_z = \frac{n_o^2}{\sqrt{n_e^2 + n_o^2}}$, Fig. 1(a). The field-induced change δn_{BU} for this BU geometry is

$$\delta n_{BU} = \frac{n_o/n_e + 1 + n_e/n_o}{6\sqrt{n_e^2 + n_o^2}} \left(\delta\tilde{\epsilon}_u + \frac{3}{2}\delta\tilde{\epsilon}_b \right) + \frac{n_e^2 - n_o^2}{\sqrt{n_e^2 + n_o^2}} (\bar{\beta} - \bar{\beta}_0). \quad (30)$$

The last term is a potential contribution of the finite pretilt angle at the boundaries. Because of the finite pretilt, the applied field can realign the director,

$$\bar{\beta}(t_{on} \leq t \leq t_{off}) = \bar{\beta}_0 \exp\left(-\frac{t - t_{on}}{\tau_{on}^F}\right), \quad (31)$$

where $\bar{\beta}_0$ is the arithmetic mean of the pretilt angles at the top and bottom plates when there is no field. After the field is switched off, the director relaxes back to the initial

state,

$$\bar{\beta}(t > t_{off}) = \bar{\beta}_0 - [\bar{\beta}_0 - \bar{\beta}(t_{off})] \exp\left(-\frac{t - t_{off}}{\tau_{off}^F}\right). \quad (32)$$

At a time scale (1–1000) ns of interest, Eq. (32) yields a practically constant value of $\bar{\beta}(t > t_{off})$.

2. Uniaxial-fluctuative geometry

Among the UF geometries determined by the condition $\sigma_{bu} = 0$ in Eq. (29), we choose the one with the incidence plane of a probing beam perpendicular to the director $\tilde{k}_z = 0$ and the incidence angle obeying the condition $\tilde{k}_y = n_o/\sqrt{2}$, Fig. 1(b). The corresponding field-induced birefringence δn_{UF} is

$$\delta n_{UF} = \frac{1}{3\sqrt{2}} \left(\frac{1}{n_o} + \frac{2}{\sqrt{2n_e^2 - n_o^2}} \right) \left(\delta\tilde{\epsilon}_u + \frac{3}{2}\delta\tilde{\epsilon}_f \right). \quad (33)$$

If the refractive indices of NLC n_e and n_o are close to the refractive index of the glass substrate n_g , then the incident angles in BU and UF geometries are close to 45° .

3. Normal geometry

In N geometry the probing light is perpendicular to the cell $\tilde{k}_y = \tilde{k}_z = 0$, and Eq. (29) reduces to

$$\delta n_N = \frac{1}{6n_o} \left(\delta\tilde{\epsilon}_u + \frac{3}{2}\delta\tilde{\epsilon}_b \right) + \frac{1}{3n_e} \left(\delta\tilde{\epsilon}_u + \frac{3}{2}\delta\tilde{\epsilon}_f \right). \quad (34)$$

III. EXPERIMENTAL METHODS

We used commercially available NLC CCN-47 (Nematel GmbH). The material parameters measured at $T = 40^\circ\text{C}$ are as follows: dielectric constants $\epsilon_{||} = 3.9$, $\epsilon_{\perp} = 9.0$, dielectric anisotropy $\Delta\epsilon = -5.1$, all determined within the field frequency range of 1–50 kHz; birefringence $\Delta n = 0.029$ at $\lambda = 633$ nm. The transverse dipole of CCN-47 molecules is large $\mu_D = 12.3 \times 10^{-30}$ C m (3.7 D) as calculated using CHEMOFFICE software. The structural formula of CCN-47 is shown in Fig. 2(a).

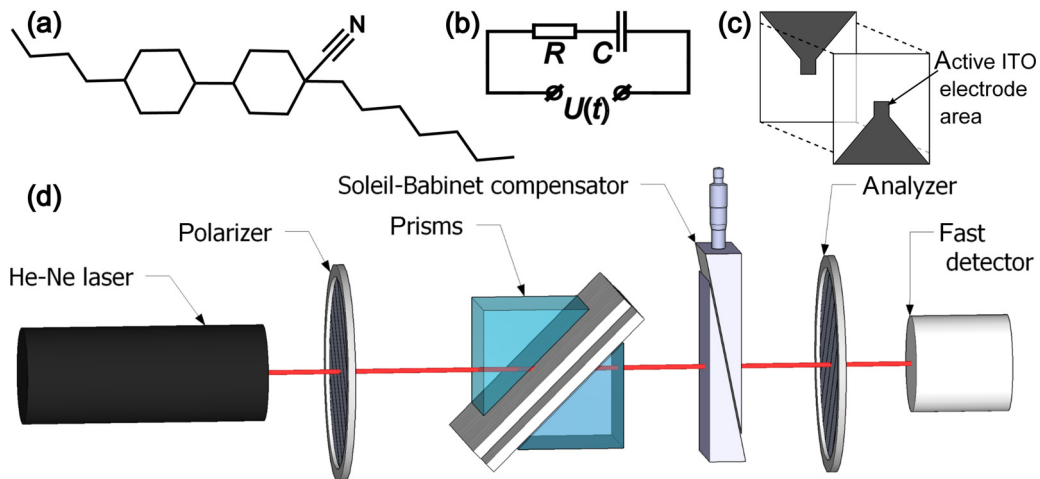


FIG. 2. (Color online) (a) Molecular structure of CCN-47. (b) Schematic RC circuit. (c) Design of cell electrodes. (d) Electro-optic setup for geometries BU and UF.

The cells were constructed from two parallel glass plates separated by spacers. The inner surfaces of these plates contain ITO electrodes and unidirectionally rubbed polyimide layers PI-2555 (HD MicroSystems), which are separated by a gap d in the range (3.5–8.2) μm . When a voltage pulse $U(t)$ is applied, an electric field $E(t)$ inside the liquid crystal is controlled by the RC circuit, Fig. 2(b), formed by the resistance R of the electrodes and the equivalent capacitance $C = C_{\text{NLC}}C_P/(C_{\text{NLC}} + C_P)$ created by the capacitances of the NLC C_{NLC} and the polymer films C_P . Most of the experiments were performed with an NLC cell of the thickness $d = 4.2 \mu\text{m}$ and the RC time $\tau_{RC} = RC = 7 \text{ ns}$. In order to reduce the RC time, we used the electrodes of low resistivity (10 Ω/square) and a small area $A_e = 3 \times 3 \text{ mm}^2$, Fig. 2(c). The dielectric constant of the polyimide PI-2555 is $\epsilon_P = 3.5$ [41]. The effective thickness for the capacitor formed by the two polymer films is $d_P = 0.2 \mu\text{m}$. The rubbing directions at the plates are parallel to each other in order to minimize the effects of nonzero pretilt. The typical pretilt angle at the used substrates was about 0.7° . To satisfy the conditions of the BU and UF geometries, Fig. 1, the NLC cell is sandwiched between two right angle glass prisms with the refractive index $n_g = 1.52$, which is close to $n_e = 1.50$ and $n_o = 1.47$ measured at $T = 40^\circ\text{C}$ and $\lambda = 633 \text{ nm}$. The temperature of the cells was controlled with an accuracy of 0.1°C by a LTS350 hot stage (Linkam Scientific Instruments) and a Linkam TMS94 controller.

The cells were tested with a He-Ne laser beam ($\lambda = 632.8 \text{ nm}$), linearly polarized along the direction that makes an angle of 45° with the incidence plane. The beam passes through the cell, the Soleil-Babinet compensator, and two crossed polarizers, Fig. 2(d). The transmitted light intensity was measured using a photodetector TIA-525 (Terahertz Technologies, response time $< 1 \text{ ns}$).

The change in light intensity caused by the applied field can be presented as

$$I(t) = [I_{\text{max}}(t) - I_{\text{min}}(t)] \sin^2 \left\{ \frac{\pi [\delta n(t) + \Delta n_{\text{eff}}] d}{\lambda} + \frac{\phi_{\text{SB}}}{2} \right\} + I_{\text{min}}(t), \quad (35)$$

where ϕ_{SB} is the variable phase retardance controlled by the Soleil-Babinet compensator and I_{min} and I_{max} are the minimum and maximum values, respectively, of the light intensity. The values of I_{min} and I_{max} are different from 0 and the ideal maximum because of parasitic effects, such as light reflection at interfaces, light scattering, and absorption. These parasitic effects might be sensitive to the applied field, which is why both I_{max} and I_{min} are shown as time dependent in Eq. (35). The role of the variable Soleil-Babinet phase difference ϕ_{SB} is to eliminate the contribution of these parasitic effects from the effects affecting the birefringence, i.e., the OPs modifications and quenching of the director fluctuations, as explained below.

The measurements are performed with two different values of the Soleil-Babinet phase retardation $\phi_A = \frac{2\pi}{\lambda}(\frac{\lambda}{4} - \Delta n_{\text{eff}}d)$ and $\phi_B = \frac{2\pi}{\lambda}(\frac{3\lambda}{4} - \Delta n_{\text{eff}}d)$. At these values, the transmitted light intensity in the field-free state is $I(t=0) = [I_{\text{max}}(0) + I_{\text{min}}(0)]/2$, Fig. 3(a), which means that the sensitivity of light intensity to the changes in optical properties is maximized. Furthermore, extraction of the useful contribution from the parasitic effects is achieved by evaluating

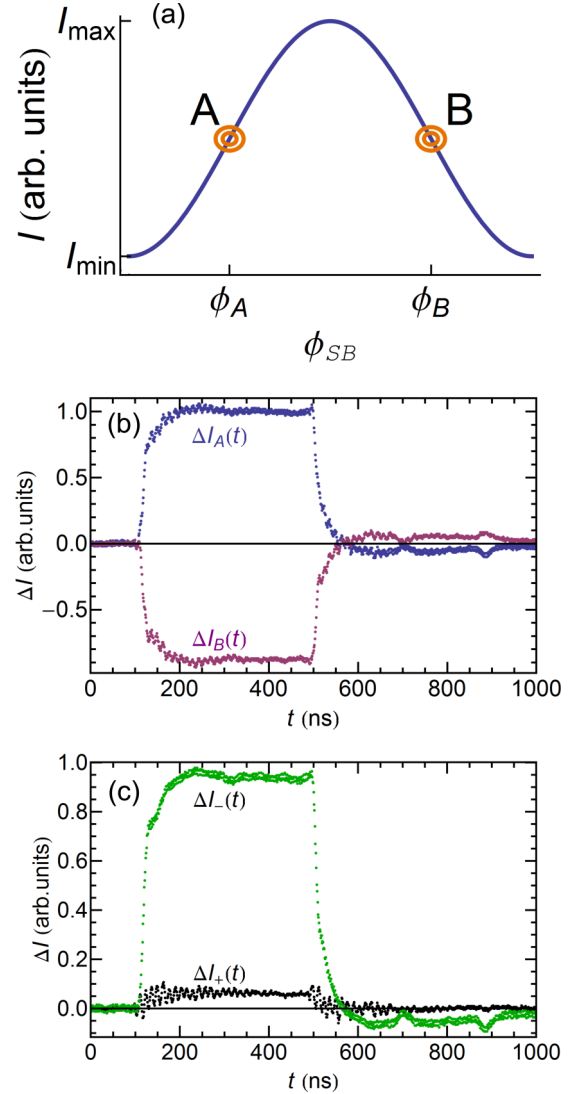


FIG. 3. (Color online) (a) Two settings of the Soleil-Babinet compensators A and B , which correspond to the maximum sensitivity of light intensity to changes in optical retardance. The two settings also allow one to separate the field-induced retardance changes from parasitic effects. (b) The optic response to $U_0 = 626 \text{ V}$ pulse measured at $T = 43^\circ\text{C}$, $d = 4.2 \mu\text{m}$ for the two settings of the compensator $\phi_{\text{SB}} = \phi_A$ and $\phi_{\text{SB}} = \phi_B$. (c) Half-difference $\Delta I_-(t)$ and half-sum $\Delta I_+(t)$ of the two optic response curves shown in (b).

the half-difference $\Delta I_-(t) = \frac{1}{2}[\Delta I_A(t) - \Delta I_B(t)] = \frac{\pi \delta n(t) d}{\lambda} [I_{\text{max}}(0) - I_{\text{min}}(0)]$ and the half-sum $\Delta I_+(t) = \frac{1}{2}[\Delta I_A(t) + \Delta I_B(t)] = \frac{1}{2}[\Delta I_{\text{max}}(t) + \Delta I_{\text{min}}(t)]$ of the optical measurements recorded for ϕ_A and ϕ_B , Figs. 3(a) and 3(c). As seen in Fig. 3(c), the half-difference $\Delta I_-(t)$ signal is significantly larger than the half-sum $\Delta I_+(t)$ signal, which indicates the prevalence of the field-induced birefringence $\delta n(t)$ effect over the parasitic factors.

Voltage pulses of amplitude U_0 up to 1 kV with nanoseconds' rise and fall fronts were produced by a pulse generator HV 1000 (Direct Energy, Inc.). The profiles of voltage pulses $U(t)$ and optic responses $I(t)$ were experimentally determined with an oscilloscope Tektronix TDS 2014 (sampling rate 1 Gsample/s).

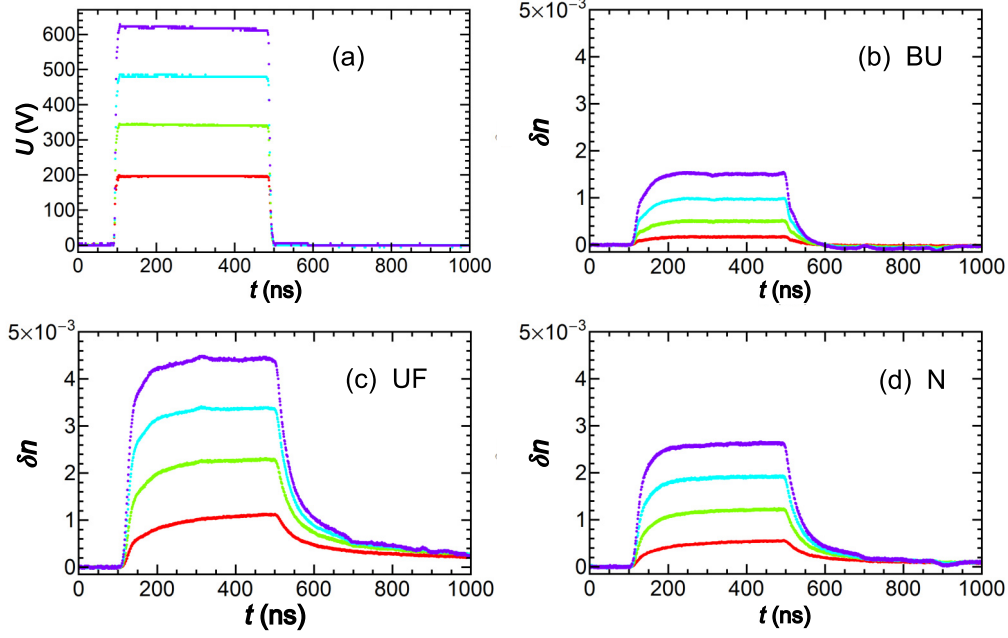


FIG. 4. (Color online) Dynamics of field-induced birefringence in geometries (b) BU, (c) UF, and (d) N in response to the applied voltage pulses (a); temperature $T = 49^\circ\text{C}$. The curves in (a)–(d) from top to bottom correspond to voltage pulses with $U_0 = 626, 484, 344,$ and 197 V, respectively.

IV. OPTIC RESPONSE DYNAMICS AND EXPERIMENTAL DATA FITTING

Short voltage pulses of duration 394 ns applied to the NLC cell, Fig. 4(a), produce the optic responses shown in Figs. 4(b)–4(d) for geometries BU, UF, and N, respectively.

In order to evaluate the dynamics of an optic response and to separate different contributions, one needs to know the profile of the voltage pulse. The latter can be presented as a sum of the exponential functions,

$$\begin{aligned} U(t < t_{\text{on}}) &= 0, \\ U(t_{\text{on}} \leq t \leq t_{\text{off}}) &= U_0(e^{-(t-t_{\text{on}})/\tau_a} - e^{-(t-t_{\text{on}})/\tau_{\text{on}}}), \\ U(t > t_{\text{off}}) &= U(t_{\text{off}})e^{-(t-t_{\text{off}})/\tau_{\text{off}}}, \end{aligned} \quad (36)$$

where t_{on} and t_{off} are the moments of time when the voltage is switched on and off, respectively; U_0 is the characteristic amplitude of the pulse applied to the electrodes of the cells, τ_{on} is the characteristic rise time of the front edge of the pulse, τ_{off} is the characteristic decay time of the rear edge of the pulse, and τ_a is the characteristic time of the slowly decaying amplitude of the pulse. The parameters U_0 , τ_a , τ_{on} , and τ_{off} are obtained by fitting the experimental profile, Fig. 5(a). It is convenient to represent the voltage pulse as a sum of the exponential functions because it allows us to solve the Kirchhoff equation

TABLE I. Coefficients a_i and v_i for exponential expansion of $E^{\text{ON}}(t)$.

i	1	2	3
a_i	$\frac{\tau_a}{\tau_a - \tau_{RC}}$	$\frac{-\tau_{\text{on}}}{\tau_{\text{on}} - \tau_{RC}}$	$\frac{-(\tau_a - \tau_{\text{on}})\tau_{RC}}{(\tau_a - \tau_{RC})(\tau_{RC} - \tau_{\text{on}})}$
v_i	$1/\tau_a$	$1/\tau_{\text{on}}$	$1/\tau_{RC}$

for an RC circuit with characteristic time τ_{RC} , which is 7 ns for the cell of thickness $4.2 \mu\text{m}$. Thus, the electric field inside the NLC $E(t < t_{\text{on}}) = 0$, $E^{\text{ON}}(t_{\text{on}} \leq t \leq t_{\text{off}})$ and $E^{\text{OFF}}(t > t_{\text{off}})$ is

$$\begin{aligned} E^{\text{ON}}(t_{\text{on}} \leq t \leq t_{\text{off}}) &= E_0 \sum_i a_i e^{-v_i(t-t_{\text{on}})}, \\ E^{\text{OFF}}(t > t_{\text{off}}) &= E^{\text{ON}}(t_{\text{off}}) \sum_j b_j e^{-\mu_j(t-t_{\text{off}})}, \end{aligned} \quad (37)$$

where $E_0 = U_0 \varepsilon_P / (\varepsilon_{\perp} d_P + \varepsilon_P d)$. In our experiment for the switching-on dynamics $t_{\text{on}} \leq t \leq t_{\text{off}}$, the summation index i runs through the values 1–3; a_i and v_i are presented in Table I. And for the switching-off dynamics $t > t_{\text{off}}$, the summation index j runs through the values 1 and 2; b_j and μ_j are presented in Table II.

The exponential form representation of $E(t)$ streamlines the fitting procedure because it allows one to evaluate Eq. (12) in an analytic form for the uniaxial $\delta\tilde{\varepsilon}_u(t)$ and biaxial $\delta\tilde{\varepsilon}_b(t)$ OPs dynamics as well as Eq. (26) for the quenching of director fluctuations $\delta\tilde{\varepsilon}_f(t)$.

A. Biaxial-uniaxial geometry fitting

The typical response of CCN-47 to the applied voltage pulse of a duration of 394 ns, recalculated in terms of the

TABLE II. Coefficients b_j and μ_j for exponential expansion of $E^{\text{OFF}}(t)$.

j	1	2
b_j	$1 - \frac{\varepsilon_P U(t_{\text{off}})}{(\varepsilon_{\perp} d_P + \varepsilon_P d) E^{\text{ON}}(t_{\text{off}})}$	$\frac{\varepsilon_P U(t_{\text{off}})}{(\varepsilon_{\perp} d_P + \varepsilon_P d) E^{\text{ON}}(t_{\text{off}})}$
μ_j	$1/\tau_{RC}$	$1/\tau_{\text{off}}$

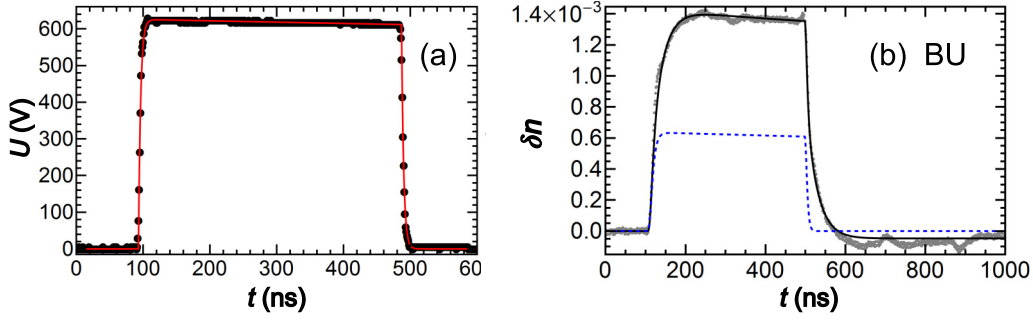


FIG. 5. (Color online) (a) Experimentally measured voltage profile fitted by Eq. (36) (solid red line) with $U_0 = 626$ V, $\tau_a = 18.5$ μ s, $\tau_{\text{on}} = 3.2$ ns, $\tau_{\text{off}} = 3.2$ ns, $t_{\text{on}} = 93$ ns, and $t_{\text{off}} = 487$ ns. (b) Optic response in BU geometry at $T = 46$ $^{\circ}$ C (gray dots) fitted with Eqs. (12), (30), (31), and (32) for one uniaxial and one biaxial mode $\tau_b = 1.95$ ns, $\tau_u = 29$ ns, $\alpha_b = 5.4 \times 10^{-20}$ m^2/V^2 , $\alpha_u = 8.9 \times 10^{-20}$ m^2/V^2 , $\tilde{\beta}_0 = 0.06^{\circ}$, and $\tau_{\text{on}}^F = 85$ ns (solid black line). The blue dashed line is the biaxial contribution.

field-induced birefringence change δn , is fitted according to Eq. (30), Fig. 5(b). The last term in Eq. (30) is the contribution due to the nonzero averaged pretilt angle $\tilde{\beta}(t)$, which is described by Eqs. (31) and (32). We extract this contribution using τ_{on}^F and considering that $\tilde{\beta}(t) = \tilde{\beta}(t_{\text{off}})$ is responsible for remaining a constant bias when in the range of 500–1000 ns, and Eq. (32) yields a practically constant value of $\tilde{\beta} = 0.1^{\circ}$. Two main contributions are the field-induced uniaxial $\delta\tilde{\epsilon}_u(t)$ and biaxial $\delta\tilde{\epsilon}_b(t)$ contributions of the NEMOP effect. Experimental data in the middle of the nematic phase fit well with the simplified model with two OPs Eq. (12), and the fitting clearly reveals two processes with substantially different relaxation times: slow in the range of tens of nanoseconds and fast in the range of nanoseconds. We assign the slow process with relaxation time $\tau_u = 28$ ns to the uniaxial OP of long axes δR_{00} and the fast process with $\tau_b = 1.95$ ns to the biaxial OP of short axes δR_{22} . This assignment is verified by the experimental results for UF geometry, discussed in the next section. Although the experimental data should be generally discussed with four OPs, the data analysis shows that it suffices to use just two different OPs and that the introduction of the third and fourth OP does not improve the fitting.

The experimental data, fitted with four parameters α_b , α_u , τ_b , and τ_u , clearly demonstrate that τ_b is the shortest time scale of the dynamic processes, being on the order of

a few nanoseconds or even shorter. For all temperatures, the fitted values of τ_b are always shorter than 2.4 ns. A more accurate determination is not possible as τ_b is at the edge of the experimental accuracy of setting and monitoring the voltage pulses. Importantly, the three other fitting parameters α_b , α_u , and τ_u show very little changes with different values of τ_b as described in Appendix A. In what follows, we set $\tau_b = 1$ ns and fit the experimental data with Eq. (30) using only three fitting parameters: τ_u , α_u , and α_b .

B. Uniaxial-fluctuative geometry fitting

The response of CCN-47 in UF geometry shown in Fig. 6(a) is obtained at the same voltage and temperature as the response in BU geometry, Fig. 5(b). The optic response has two contributions in Eq. (33): the modification of the uniaxial OP and the quenching of director fluctuations. The contribution of the director fluctuations described by Eq. (26) can be simplified for our fitting procedure because $\tau_d \approx 60$ ms for the cell thickness 4.2 μ m and $\tau_c < 10$ ns for $q_c \approx 1$ nm^{-1} . Therefore, the term inside the curly brackets in Eq. (26) is close to unity and

$$\delta\tilde{\epsilon}_f(t) = A \frac{e^{-S(t)}}{\sqrt{\gamma_{\text{eff}}}} \int_0^t \frac{f_E(t')}{\sqrt{(t-t')}} e^{S(t')} dt', \quad (38)$$

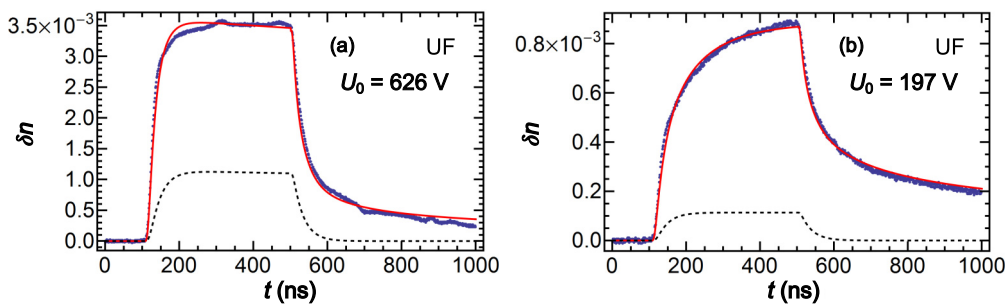


FIG. 6. (Color online) Optic response measured in UF geometry at 46 $^{\circ}$ C. Uniaxial component $\delta\tilde{\epsilon}_u(t)$ parameters α_u and τ_u obtained from BU geometry at voltage U_0 were used to fit UF geometry data and to obtain A and γ_{eff} . (a) $\alpha_u = 9.5 \times 10^{-20}$ m^2/V^2 and $\tau_u = 28$ ns for the applied voltage pulse $U_0 = 626$ V yield parameters $A = 1.7$ μ s (m/kg) $^{1/2}$ and $\gamma_{\text{eff}} = 25$ mPa s. (b) $\alpha_u = 9.6 \times 10^{-20}$ m^2/V^2 and $\tau_u = 30$ ns for $U_0 = 197$ V pulse yield $A = 1.7$ μ s (m/kg) $^{1/2}$ and $\gamma_{\text{eff}} = 15$ mPa s. The experimental points are fitted with our model (solid red line), and the dashed line is the uniaxial contribution $\delta\tilde{\epsilon}_u(t)$, obtained from BU geometry.

where A and γ_{eff} are the fitting parameters. Substituting Eq. (37) into Eq. (38), we represent $\delta\tilde{\varepsilon}_f(t)$ by two analytical expressions: switching-on dynamics $\delta\tilde{\varepsilon}_f^{\text{ON}}(t_{\text{on}} \leq t \leq t_{\text{off}})$ and the switching-off dynamics $\delta\tilde{\varepsilon}_f^{\text{OFF}}(t > t_{\text{off}})$ (see Appendix B for details). The switching-on fluctuations dynamics is

$$\begin{aligned} \delta\tilde{\varepsilon}_f^{\text{ON}}(t_{\text{on}} \leq t \leq t_{\text{off}}) &= A \frac{f_0 e^{-2\nu_1(t-t_{\text{on}})}}{\sqrt{\gamma_{\text{eff}}}} \left[a_1^2 \sqrt{\pi} \bar{\tau}_f \text{erf}\left(\sqrt{\frac{t-t_{\text{on}}}{\bar{\tau}_f}}\right) \right. \\ &\quad \left. + 2e^{-(t-t_{\text{on}})/\bar{\tau}_f} \sum_{i,i'=1}^3 a_i a_{i'} \frac{D(\sqrt{\lambda_{ii'}(t-t_{\text{on}})})}{\sqrt{\lambda_{ii'}}} \right], \quad (39) \end{aligned}$$

$$\begin{aligned} \delta\tilde{\varepsilon}_f^{\text{OFF}}(t > t_{\text{off}}) &= A \frac{f_0 \sqrt{\pi}}{\sqrt{\gamma_{\text{eff}}}} \left(a_1^2 g e^{-2\nu_1(t_{\text{off}}-t_{\text{on}})} \sqrt{\bar{\tau}_f} e^{(t-t_{\text{off}})/\bar{\tau}_f} \left[\text{erf}\sqrt{\frac{t-t_{\text{on}}}{\bar{\tau}_f}} - \text{erf}\sqrt{\frac{t-t_{\text{off}}}{\bar{\tau}_f}} \right] \right. \\ &\quad \left. + \frac{2}{\sqrt{\pi}} g \sum_{i,i'=1}^3 a_i a_{i'} \frac{1}{\sqrt{\lambda_{ii'}}} \{ e^{-a_1^2(t_{\text{off}}-t_{\text{on}})/\tau_f} D(\sqrt{\lambda_{ii'}(t-t_{\text{on}})}) - e^{-(\nu_i+\nu_{i'})(t_{\text{off}}-t_{\text{on}})} D(\sqrt{\lambda_{ii'}(t-t_{\text{off}})}) \} \right. \\ &\quad \left. + \frac{f_E^{\text{ON}}(t_{\text{off}})}{f_0} \frac{2}{\sqrt{\pi}} \sum_{j,j'=1}^2 \frac{b_j b_{j'}}{\sqrt{\mu_j + \mu_{j'}}} D(\sqrt{(\mu_j + \mu_{j'})(t-t_{\text{off}})}) \right), \quad (40) \end{aligned}$$

where $g = \exp\left[-\frac{f_E^{\text{ON}}(t_{\text{off}})}{\gamma_{\text{eff}}} \sum_{j,j'=1}^2 \frac{b_j b_{j'}}{\mu_j + \mu_{j'}}\right]$.

Fitting the experimental data with the corresponding Eqs. (12), (39) and (40) reveals that the characteristic time of the fastest process is about 30 ns, and there is no process with the characteristic time on the order of 1 ns, which we observe in BU geometry, Fig. 5(b). Therefore, the UF experiment proves our earlier assignment that the relatively slow (30 ns) process in BU geometry is related to the modification of the uniaxial OP and the fast nanosecond process is caused by the induced biaxial OP.

The reliable fitting of the uniaxial and fluctuations contributions with Eqs. (12), (39), and (40) might be challenging, especially for higher electric fields, when the characteristic times $\bar{\tau}_f$ and τ_u are on the same order. On the other hand, τ_b and τ_u are more than one order of magnitude different, and fitting BU geometry allows us to obtain the biaxial and uniaxial contributions with high accuracy. Therefore, we separate the uniaxial contribution from the experimental data in UF geometry using the corresponding fitting parameters α_u and τ_u obtained from BU geometry for the same temperature and voltage pulse. Then we fit the remaining part corresponding to the director fluctuations with Eqs. (39) and (40). Although we use only two fitting parameters A and γ_{eff} , the experimental data fit for UF geometry is encouraging, both for higher electric fields when the optic response is faster, Fig. 6(a) and for lower fields when the response is slower, Fig. 6(b).

C. Normal geometry

Using an arbitrary direction of the probing beam propagation in our experimental system, one can obtain a linear combination of two independent experimental sets of data Eq. (29). More specifically, the optic response in N geometry

where $\sum_{i,i'=1}^3$ is the sum with the term $i = i' = 1$ being excluded; $f_0 = \varepsilon_0 |\Delta\varepsilon| E_0^2$; $\lambda_{ii'} = \nu_i + \nu_{i'} - a_1^2/\tau_f$; $\tau_f = \gamma_{\text{eff}}/f_0$; $\bar{\tau}_f = |\lambda_{11}|^{-1} = \tau_f/(a_1^2 - 2\tau_f\nu_1)$ is the characteristic time for the dynamics of fluctuations' quenching; and $D(z) = e^{-z^2} \int_0^z e^{t^2} dt$ is Dawson's integral; see Chap. 7 in Ref. [40].

In Eq. (39), the first term with the error function provides the main contribution, whereas the terms with Dawson's integrals describe small corrections caused by the nonsquare shape of the electric pulse in the NLC. In the case of an ideal square electric pulse, $\tau_a \rightarrow \infty$, $\tau_{\text{on}} \rightarrow 0$, and $\tau_{RC} \rightarrow 0$, the terms with Dawson's integrals disappear, and $\bar{\tau}_f = \tau_f$.

The switching-off dynamics is

can be presented as the linear combination of respective responses in BU and UF geometries. In order to validate the two experimental sets of data taken in BU and UF geometries, we perform an experiment in N geometry.

With a probing beam impinging normal on the substrates, N geometry contains the contributions of all three processes Eq. (34): the field-enhanced uniaxial OP, field-induced biaxial OP, and the quenching of director fluctuations. Equations (30), (33), and (34) show that the linear combination of the optic responses in BU, UF, and N geometries expressed as

$$\begin{aligned} \delta n_0(t) &= \delta n_N(t) - \frac{\sqrt{n_e^2 + n_o^2}}{n_o/n_e + n_o + n_e} \left[\delta n_{\text{BU}}(t) \right. \\ &\quad \left. - \frac{n_e^2 - n_o^2}{\sqrt{n_e^2 + n_o^2}} (\beta - \beta_0) \right] \\ &\quad - \frac{\sqrt{2}n_o\sqrt{2n_e^2 - n_o^2}}{n_e(\sqrt{2n_e^2 - n_o^2} + 2n_o)} \delta n_{\text{UF}}(t) \quad (41) \end{aligned}$$

should be zero. This quantity can be used as an estimate of the experimental error. In all our experiments, the field-induced phase difference $\delta n_0(t)$, described in Eq. (41), deviates from zero by no more than 1.4×10^{-4} (except at the moments of time corresponding to the front and rear edges of the voltage pulse), Fig. 7.

V. DISCUSSION

A. Biaxial-uniaxial geometry

The experimental data follow our model fairly well, Figs. 5(b) and 13(a). In particular, at the temperatures

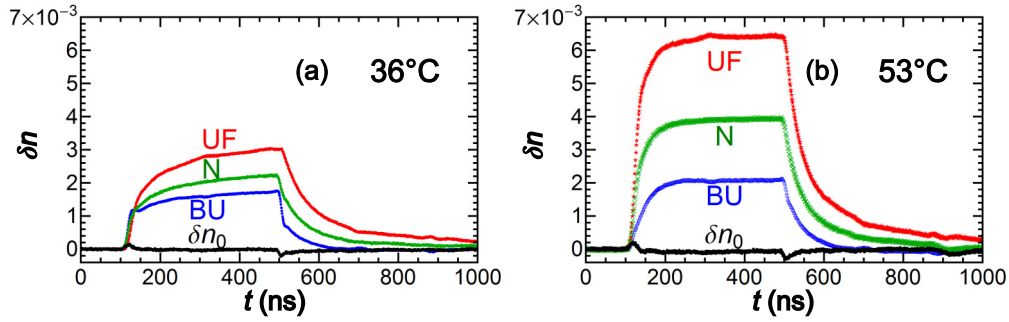


FIG. 7. (Color online) Optic responses measured in geometries BU, UF, and N at (a) 36 °C and (b) 53 °C. The lowest black curve corresponds to $\delta n_0(t)$ defined in Eq. (41). Applied voltage pulse $U_0 = 626$ V.

$T = 31, 46,$ and 49 °C, Fig. 8, that are far from the nematic-to-isotropic ($T_{NI} = 56.5$ °C) phase transition, the fitting parameters, namely, the biaxial α_b and uniaxial α_u susceptibilities and the characteristic uniaxial time τ_u , do not depend on the electric field as expected, see Eq. (12). Close to T_{NI} at $T = 54$ °C, α_u and τ_u decrease, whereas α_b increases with the electric field. Such a behavior in the pretransitional region might be attributed to the following factors. First, we restrict our model by the second-order term of the free energy density expansion Eq. (4). One can expect that near the T_{NI} , the higher-order terms should be taken into account. Second, although our model describes the NEMOP effect through four OPs Eq. (11), we fit experimental data with the assumption of only two OPs being significant (R_{00} and R_{22}) Eq. (12).

The temperature dependences of α_u and τ_u , shown in Fig. 9, are obtained for $E_0 = 74$ V/ μ m. Such a field is not very strong, yet the induced optic response is sufficiently large to provide reasonable accuracy.

When the temperature approaches T_{NI} , both the uniaxial susceptibility α_u and the relaxation time τ_u increase, Fig. 9(a). In the theory, both quantities are inversely proportional to $\partial^2 f_m / \partial R_{jk} \partial R_{jk}$, see Eq. (4), i.e., $\alpha_u \propto 1/M_{00,00}$ and $\tau_u \propto 1/M_{00,00}$. The experimentally observed increase in α_u and τ_u is, thus, explained by the flattening of the free energy

density profile as a function of R_{00} near the phase transition temperature. Therefore, the experimental behavior of α_u and τ_u is consistent with the Landau-Khalatnikov description close to the phase transition [34].

The reciprocal quantities $1/\alpha_u$ and $1/\tau_u$ demonstrate a quasilinear behavior at both low and high temperatures of the nematic range, Fig. 9(b). Close to T_{NI} , this behavior could be explained by the Landau-de Gennes theory for the nematic phase, where $M_{00,00}$ has a quasilinear temperature dependence and adopts a zero value at the absolute temperature limit T^{**} of overheating of the nematic phase, Fig. 9(b).

At the lower temperature limit of the nematic phase, the value of α_u slightly increases, Fig. 9(b), which could be attributed to the formation of fluctuative smectic clusters near the nematic-to-smectic phase transition, which is enhanced by the electric field. Clusters might also explain the increase in the response time τ_u at the low temperatures.

The biaxial susceptibility α_b shows a well-pronounced increase as the temperature is lowered, Fig. 10(a), which can be explained in the following way. In our model, α_b is proportional to $M_{22,22}^{-1}$ Eq. (13). According to the Landau theory, the biaxial second-order coefficient $M_{22,22}$ in the uniaxial phase Eq. (4) has to go to zero at the temperature T_{ub} of the uniaxial-biaxial nematic phase transition, and this

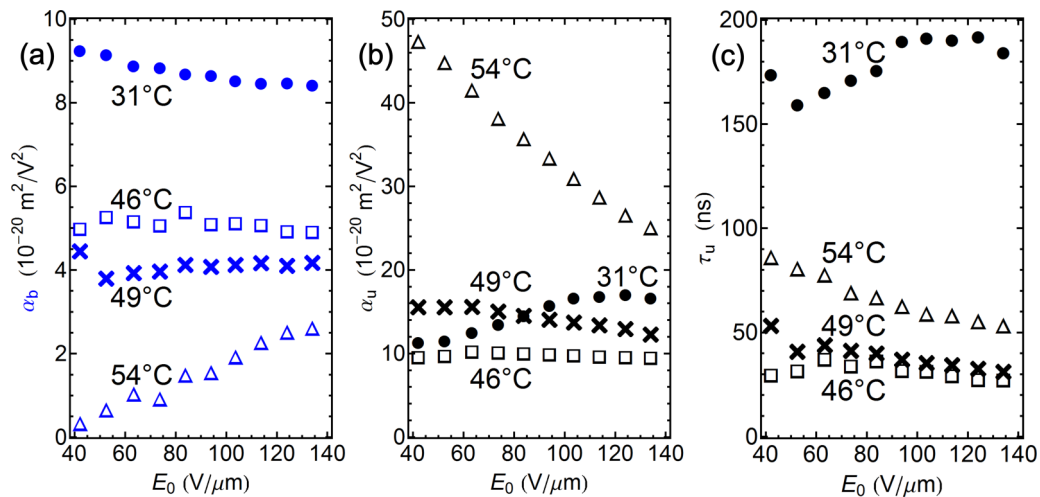


FIG. 8. (Color online) Electric-field dependence of (a) biaxial α_b , (b) uniaxial α_u susceptibilities, and (c) uniaxial time τ_u at different temperatures: 31 °C (●), 46 °C (□), 49 °C (×), and 54 °C (Δ).

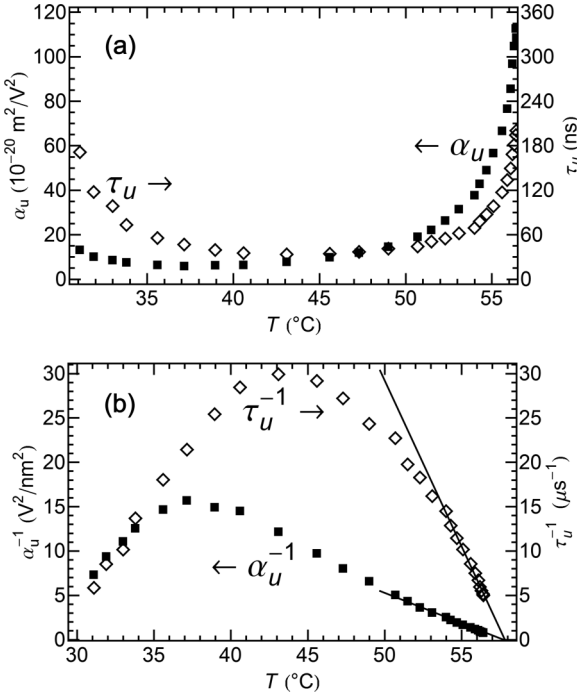


FIG. 9. Temperature dependences of (a) uniaxial susceptibility α_u (■) and uniaxial characteristic time τ_u (◇) measured at $E_0 = 74 \text{ V}/\mu\text{m}$ and (b) their reciprocal values α_u^{-1} and τ_u^{-1} fitted with straight lines.

dependence is linear $M_{22,22} \propto (T - T_{\text{ub}})$. Therefore, one can expect that $\alpha_b^{-1} \propto (T - T_{\text{ub}})$ and the experimental data show such a linear dependence for temperatures far below T_{NI} , Fig. 10(b). The slope of the linear temperature dependence of α_b^{-1} shows that the hypothetical uniaxial-to-biaxial nematic phase transition temperature is $T_{\text{ub}} = 5 \text{ }^\circ\text{C}$, Fig. 10(b). This temperature is well below the uniaxial-to-smectic A transition temperature $T_{\text{NA}} = 30 \text{ }^\circ\text{C}$ observed for CCN-47. Thus, the molecular structure of CCN-47 is not conducive for the search of a biaxial nematic phase. On a general note, the temperature dependence of α_b can serve as an indicator of how close a uniaxial nematic material might be to forming a biaxial nematic phase in the absence of the external electric field.

B. Uniaxial-fluctuative geometry

This geometry offers a convenient way for analyzing the nanosecond dynamics of the quenching of director fluctuations because the biaxial contribution is absent and the uniaxial contribution in Eq. (33) can be separated from the fluctuative contribution since the values of α_u and τ_u are already known from the fit of the experimental data in BU geometry. The electric-field dependences of the fitting parameters A and γ_{eff} for several temperatures are shown in Fig. 11. As expected, the amplitude coefficient A , describing the changes in the optic tensor caused by the quenching of director fluctuations Eq. (26), remains almost field independent and increases with temperature, Figs. 11(a) and 12. However, the value of A is about two times bigger than the value expected from its definition in Eq. (26), calculated with the known elastic constants [42] and the measured $n_e = 1.50$ and $n_o = 1.47$.

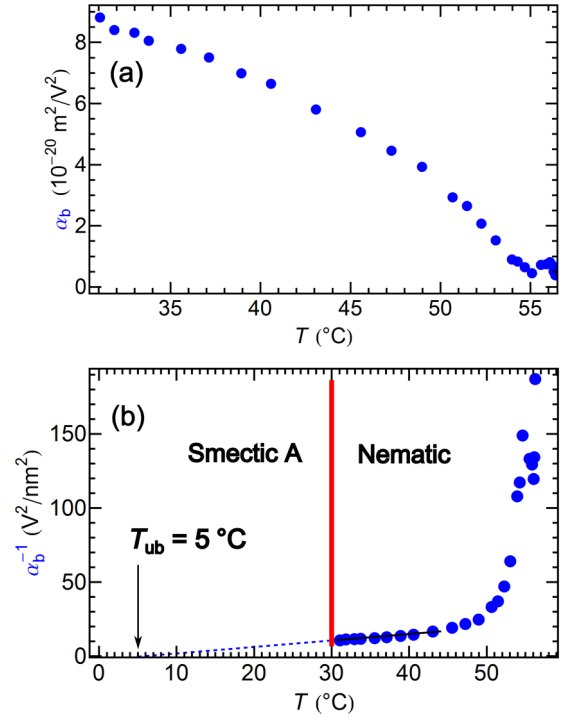


FIG. 10. (Color online) Temperature dependences of (a) biaxial susceptibility α_b (●) and (b) its reciprocal α_b^{-1} fitted with a straight line.

The obtained effective viscosity γ_{eff} demonstrates a weak monotonous increase with the electric field, Fig. 11(b) and is slightly smaller than the macroscopic viscosities of CCN-47 homolog compounds and their mixtures [43]. As expected, in the nematic phase, γ_{eff} increases with a decrease in temperature, Fig. 12. The increase is especially pronounced near the transition to the smectic A phase. The latter can be attributed to the pretransitional phenomena, such as fluctuative cybotactic smectic clusters.

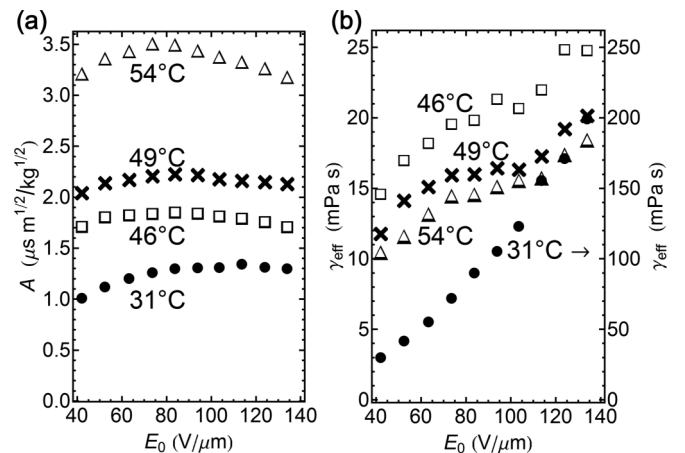


FIG. 11. Fitting parameters (a) A and (b) γ_{eff} obtained from experimental data at $31 \text{ }^\circ\text{C}$ (●), $46 \text{ }^\circ\text{C}$ (□), $49 \text{ }^\circ\text{C}$ (×), and $54 \text{ }^\circ\text{C}$ (△).

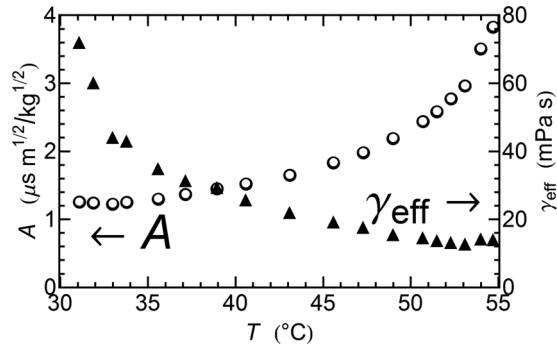


FIG. 12. Temperature dependence of A (\circ) and γ_{eff} (\blacktriangle) at $E_0 = 74 \text{ V}/\mu\text{m}$.

VI. CONCLUSION

In this paper, we explored both theoretically and experimentally the electro-optic response of an NLC cell in which the electric field does not cause director reorientation. We demonstrated three mechanisms contributing to the field-induced change in optical birefringence: nanosecond electric modification of (a) biaxial, (b) uniaxial OPs, and (c) quenching of the director fluctuations. Our observations reveal that these mechanisms have different characteristic times. For CCN-47, these times are (a) less than 2 ns for the biaxial NEMOP, (b) tens of nanoseconds for the uniaxial NEMOP, and (c) a wide range of characteristic times from tens of nanoseconds to milliseconds for the quenching of director fluctuations.

We developed a model of the NEMOP effect using two uniaxial and two biaxial nematic OPs. Their dynamics are described by two uniaxial and two biaxial modes Eq. (5). We used a simplified two-mode version of the model to fit our experimental data for CCN-47; the uniaxial OP of the long molecular axes and the biaxial OP of the short molecular axes appear to be the dominant OPs for this material.

We describe the dynamics of director fluctuations using the macroscopic viscoelastic approach Eq. (20) with Frank-Oseen elastic energy in splay-twist one-constant approximation $K_1 = K_2$ and with a constant effective viscosity. Within these approximations, we derived the contribution for the quenching of director fluctuations to the field-induced modifications of the optic tensor Eq. (26).

Experimentally, we determine the field-induced changes in the effective birefringence δn_{eff} , which contains the uniaxial $\delta \tilde{\epsilon}_u$, biaxial $\delta \tilde{\epsilon}_b$, and fluctuational $\delta \tilde{\epsilon}_f$ contributions Eq. (29). In order to separate these contributions, we used the so-called BU and UF geometries in which one of the three contributions is nullified. We also independently validated the separation of different mechanisms by measuring the optic response in normal incidence (N) geometry, Fig. 7.

In BU geometry, with no contribution from the fluctuations quenching, the dynamics of the electro-optic response develops over time scales of nanoseconds and is well described by two different characteristic times τ_u (tens of nanoseconds) and τ_b (about 2 ns or less). We associate these characteristic times with the uniaxial and biaxial modifications, respectively, of the optic tensor, see Eqs. (30) and (12). The assignment of the fastest relaxation time τ_b to the biaxial modification is justified by the measurements in UF geometry in which

the nanosecond relaxation is absent. The biaxial susceptibility shows a strong temperature dependence at low temperatures $\alpha_b \propto (T - T_{\text{ub}})^{-1}$, which indicates a possible phase transition from the uniaxial to the biaxial nematic phase in a field-free state at some temperature T_{ub} . The extrapolated value is $T_{\text{ub}} = 5 \text{ }^\circ\text{C}$, much lower than the temperature $30 \text{ }^\circ\text{C}$ of the actual phase transition from the uniaxial nematic to the smectic A phase. Therefore, in the explored material CCN-47, the hypothetical biaxial nematic state is suppressed by the occurrence of the smectic A phase. A similar test can be used to find T_{ub} in other materials in order to facilitate the search for potential biaxial nematics.

UF geometry provides interesting information about the behavior of director fluctuations on nanoseconds' time scales. In this geometry, the biaxial modifications in the optic tensor $\delta \tilde{\epsilon}_b$ are eliminated, and the uniaxial changes can be evaluated by employing the values of parameters α_u and τ_u obtained from the slow component of the BU response. The remaining changes $\delta \tilde{\epsilon}_f$ in the optic tensor can be attributed to the quenching of director fluctuations. The director fluctuations model provides a good fit to the experimental optic response, Fig. 6. As expected, the amplitude of director fluctuations grows with temperature, whereas the effective viscosity decreases with temperature, Fig. 12. The amplitude coefficient A does not depend on the electric field but is bigger than theoretically expected, Fig. 11(a), which can be attributed to the simplifying assumptions of the theory. The most intriguing feature is that the effective viscosity increases with the field, Fig. 11(b), thus, possibly indicating that the classic viscoelastic theory with constant material parameters might approach its limit of validity when applied to the nanoseconds dynamics in strong electric fields.

The presented NEMOP effect should be distinguished from the classic Kerr effect. The Kerr effect consists of field-induced birefringence emerging in the otherwise isotropic fluid. It is an essentially uniaxial effect with the induced optic axis being always parallel to the applied field. The Kerr effect can be observed in nonmesogenic fluids [44–46] and in the isotropic phase of mesogenic compounds [47–52]. In the first case, the effect is practically temperature independent, whereas in the second case, it shows a strong enhancement near the isotropic-to-nematic phase transition [50,52]. In comparison, the NEMOP response of CCN-47 with a negative dielectric anisotropy features both uniaxial and biaxial optical changes. The biaxial changes are faster than the uniaxial changes at the same temperature and in the same electric field as discussed above. Similar to the case of electro-optic effects in uniaxial and biaxial nematics [53], one could expect that the biaxial part of NEMOP would be generally faster than the uniaxial part. It is also expected that as the relative contributions of the biaxial and uniaxial change, the amplitude and relaxation times of these changes would be strongly dependent on the molecular structure as the NEMOP effect is essentially a molecular-scale phenomenon. Indeed, our recent results [13] demonstrate that different mesogenic materials show very different amplitudes of the field-induced NEMOP birefringence that exceed the data presented for CCN-47 by at least one order of magnitude.

From the fundamental point of view, NEMOP represents an opportunity to analyze the complex uniaxial-biaxial response of the orientationally ordered medium to the applied electric

field on the scale of nanoseconds. In this paper, we explored only one material. Further studies should expand to materials with different molecular structures and material parameters. For instance, the NEMOP effect can be observed not only in materials with a negative dielectric anisotropy as is the case of CCN-47, but also in materials with positive dielectric anisotropy. It would be of interest to compare the parameters of the NEMOP effect to the parameters of the Kerr effect in the isotropic phase of the same compound. These studies would shed some light on which mode of optic response would be the most beneficial for the nanosecond electro-optic applications.

ACKNOWLEDGEMENTS

We thank M. Groom and C. Culbreath for their help with the experimental setup. The work was supported by DOE Grant No. DE-FG02-06ER 46331 (measurements of the optic response and theory), NSF Grant No. DMR-1410378, the State of Ohio through the Ohio Development Services Agency, and the Ohio Third Frontier Grant No. TEGC20140133 (analysis of the field and temperature dependences of the optic response). B.-X.L. acknowledges the China Scholarship Council and the Jiangsu Innovation Program for Graduate Education Grant No. CXLX13_155 for support.

APPENDIX A: FITTING PROCEDURE FOR BIAxIAL-UNIAXIAL GEOMETRY

In this appendix, we explain the procedure to fit the experimental data obtained in BU geometry. There are three processes that are relevant in the dynamics of optic response in

this geometry, namely, director reorientation associated with the finite pretilt and biaxial and uniaxial changes in the OPs.

The slowest one is the dynamics of the pretilt angle $\bar{\beta}(t)$, described by Eqs. (31) and (32). When the field is switched on, the characteristic time $\tau_{\text{on}}^F \approx \gamma_1/(\epsilon_0|\Delta\epsilon|E^2)$ of the pretilt dynamics with $\gamma_1 \approx 0.1$ Pa s being the rotational viscosity and $E \approx 2 \times 10^8$ V/m being the typical electric field is about 100 ns, which is longer than the rate of uniaxial and biaxial changes $\tau_u \sim 30$ and $\tau_b < 2$ ns. When the electric field is switched off at $t = t_{\text{off}}$, the relaxation time of the pretilt angle becomes even longer $\tau_{\text{off}}^F \approx \gamma_1 d^2/(\pi^2 K_1) \sim 10$ ms. At the scale of nanoseconds relevant to our experiments, this extremely slow relaxation yields a practically time-independent contribution to the overall optical signal that reveals itself in Fig. 13(a) as a negative-valued “tail” in the time dependence of δn [see also Figs. 3(c) and 5(b)]. Since the uniaxial and biaxial modifications relax much faster than the pretilt angle, we use the optic signal measured at $t > t_{\text{off}} + 500$ ns to determine the value of $\bar{\beta}(t > t_{\text{off}})$; the value of $\bar{\beta}_0$ follows from Eq. (31). Note that the overall effect of $\bar{\beta}(t)$ is small, contributing less than 5% to the optic response.

After the exclusion of the pretilt angle contribution, the remaining dynamics is associated with the uniaxial and biaxial changes in the OPs that occur on short time scales (1–100) ns. We fit the experimental data with Eq. (30) in which $\bar{\beta}(t)$ is defined as explained above. The fitting is performed through minimization of the residuals function,

$$\text{var} = \frac{1}{N-4} \sum_{i=1}^N [\delta n(t_i) - \delta n_{\text{BU}}(t_i, \alpha_u, \alpha_b, \tau_u, \tau_b)]^2, \quad (\text{A1})$$

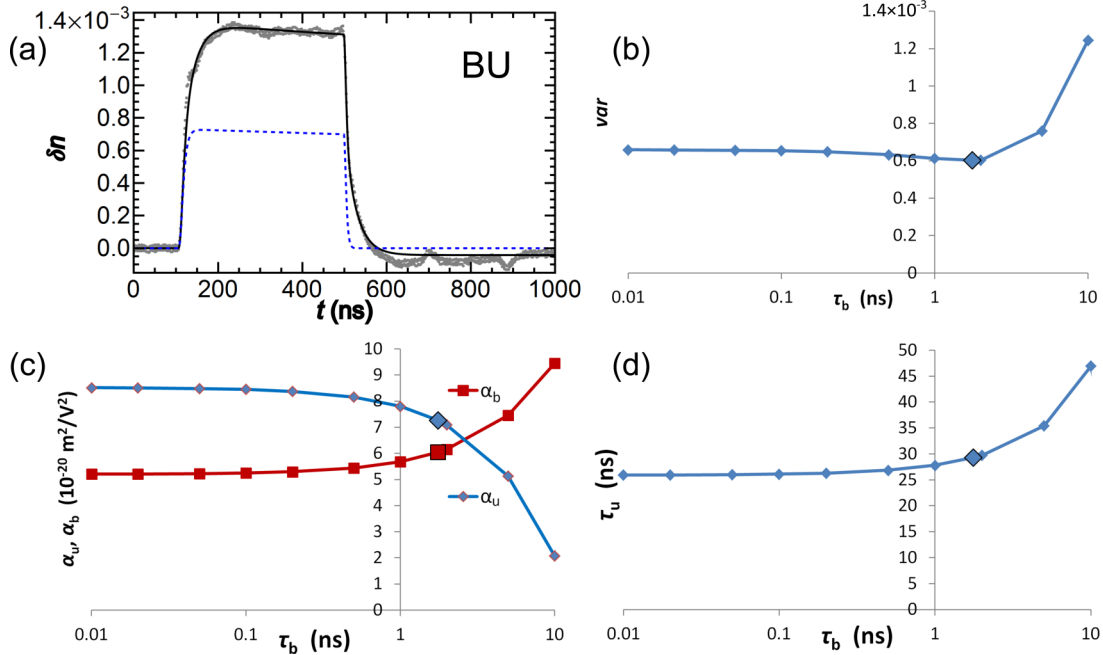


FIG. 13. (Color online) (a) Optic response at $T = 43$ °C (gray dots) fitted with Eq. (30) for one uniaxial and one biaxial mode, $\tau_b = 1.76$ ns, $\tau_u = 31$ ns, $\alpha_b = 5.8 \times 10^{-20}$ m²/V², and $\alpha_u = 8.0 \times 10^{-20}$ m²/V² (solid black line). The blue dashed line is the biaxial contribution. (b) Dependence of the residuals function on the preselected value of τ_b , obtained from the fitting of the optic response at $T = 43$ °C, $U_0 = 626$ V with Eq. (30). Dependence of the fitted values of (c) α_u , α_b and (d) τ_u on the preselected value of τ_b . The big marker on the plots corresponds to $\tau_b = 1.76$ ns, obtained as a free fitting parameter.

where N is the number of experimental data points $\{t_i, \delta n(t_i)\}$ and δn_{BU} is the fitting function as defined in Eq. (30).

The fitting clearly reveals two different relaxation processes with substantially different relaxation times: τ_u in the range of tens of nanoseconds and τ_b in the range of nanoseconds. For example, the optic response to the voltage $U_0 = 626$ V yields $\tau_b = 1.8$ and $\tau_u = 31$ ns, Fig. 13(a). As long as τ_b is less than 2 ns, the fitting produces practically the same values of the three other parameters, α_u , α_b , and τ_u , Figs. 13(b)–13(d).

APPENDIX B: ANALYTIC DESCRIPTION OF THE DYNAMICS OF DIRECTOR FLUCTUATIONS QUENCHING

In this appendix, we derive an expression for the dynamics of the fluctuative contribution described by Eq. (38). To simplify derivation we set $t_{\text{on}} = 0$. The function $f_E(t) = \varepsilon_0 |\Delta \varepsilon| E^2(t)$ reads from Eq. (37) as

$$f_E^{\text{ON}}(t \leq t_{\text{off}}) = f_0 \sum_{i,i'=1}^3 a_i a_{i'} e^{-(v_i+v_{i'})t},$$

$$f_E^{\text{OFF}}(t > t_{\text{off}}) = f_E^{\text{ON}}(t_{\text{off}}) \sum_{j,j'=1}^2 b_j b_{j'} e^{-(\mu_j+\mu_{j'})(t-t_{\text{off}})}, \quad (\text{B1})$$

where $f_0 = \varepsilon_0 |\Delta \varepsilon| E_0^2$, $E_0 = U_0 \varepsilon_P / (\varepsilon_{\perp} d_P + \varepsilon_P d)$ is the characteristic amplitude of the electric field inside the NLC Eq. (37), $i = 1-3$, see Table I of the main text, and $j = 1, 2$, see Table II.

For the switching-on process, $t \leq t_{\text{off}}$, $S^{\text{ON}}(t \leq t_{\text{off}}) = \frac{1}{\gamma_{\text{eff}}} \int_0^t f_E^{\text{ON}}(t') dt'$, therefore, $\exp[S^{\text{ON}}(t)]$ in Eq. (38) can be presented in a form $\exp[S^{\text{ON}}(t)] = \prod_{i,i'=1}^3 P_{ii'}(t)$, where $P_{ii'}(t) = \exp[\frac{a_i a_{i'}}{\tau_f (v_i + v_{i'})} (1 - e^{-(v_i + v_{i'})t})]$ and $\tau_f = \gamma_{\text{eff}} / f_0$. One can see from Table I that $|a_i| \sim 1$ and v_i satisfy the conditions $v_1 \tau_f \ll 1$ and $v_i \tau_f \gg 1$ for $i = 2, 3$. Thus, the exponential term in parentheses can be expanded for $P_{11}(t) = \exp(a_1^2 t / \tau_f)$ and neglected for all other terms $P_{ii'} = \exp[\frac{a_i a_{i'}}{\tau_f (v_i + v_{i'})}]$. Therefore, Eq. (38) can be presented as

$$\delta \tilde{\varepsilon}_f^{\text{ON}}(t \leq t_{\text{off}}) = A \sqrt{\pi} \frac{f_0}{\sqrt{\gamma_{\text{eff}}}} e^{-a_1^2 t / \tau_f} \sum_{i,i'=1}^3 a_i a_{i'} I(\lambda_{ii'}, 0, t), \quad (\text{B2})$$

where $\lambda_{ii'} = v_i + v_{i'} - \frac{a_i^2}{\tau_f}$ and $I(\lambda, t_0, t) = \int_{t_0}^t \frac{e^{-\lambda t'}}{\sqrt{t-t'}} dt'$. The integral $I(\lambda, t_0, t)$ yields either the error function or Dawson's integral, see, e.g., Chaps. 5 and 7 of Ref. [40],

$$I(\lambda, t_0, t) = \begin{cases} \sqrt{\pi} \frac{e^{|\lambda|t}}{\sqrt{|\lambda|}} \text{erf} \sqrt{|\lambda|(t-t_0)}, & \text{if } \lambda < 0, \\ 2 \frac{e^{-\lambda t_0}}{\sqrt{\lambda}} D(\sqrt{\lambda(t-t_0)}), & \text{if } \lambda > 0. \end{cases} \quad (\text{B3})$$

One can see from Table I that $\lambda_{11} < 0$ and $\lambda_{ii'} > 0$ for all other cases; thus, Eq. (38) for the switch-on dynamics $t \leq t_{\text{off}}$

becomes

$$\delta \tilde{\varepsilon}_f^{\text{ON}}(t \leq t_{\text{off}}) = A \frac{f_0}{\sqrt{\gamma_{\text{eff}}}} e^{-a_1^2 t / \tau_f} \left[\sqrt{\pi} \frac{a_1^2 e^{|\lambda_{11}|t}}{\sqrt{|\lambda_{11}|}} \text{erf} \sqrt{|\lambda_{11}|t} + 2 \sum_{i,i'=1}^3 \frac{a_i a_{i'}}{\sqrt{\lambda_{ii'}}} D(\sqrt{\lambda_{ii'} t}) \right], \quad (\text{B4})$$

where $\sum_{i,i'=1}^3$ is the sum with the term $i = i' = 1$ being excluded. Equation (B4) is presented as Eq. (39) in the main text.

For the switching-off process $t > t_{\text{off}}$, we can split $S(t > t_{\text{off}})$ into two parts $S(t > t_{\text{off}}) = S^{\text{ON}}(t_{\text{off}}) + S^{\text{OFF}}(t > t_{\text{off}})$, where

$$S^{\text{OFF}}(t > t_{\text{off}}) = \frac{1}{\gamma_{\text{eff}}} \int_{t_{\text{off}}}^t f_E^{\text{OFF}}(t') dt'$$

$$= \frac{f_E^{\text{ON}}(t_{\text{off}})}{\gamma_{\text{eff}}} \sum_{j,j'=1}^2 \frac{b_j b_{j'}}{(\mu_j + \mu_{j'})} \times (1 - e^{-(\mu_j + \mu_{j'})(t-t_{\text{off}})}). \quad (\text{B5})$$

Thus, Eq. (38) is also divided into two parts,

$$\delta \tilde{\varepsilon}_f^{\text{OFF}}(t > t_{\text{off}}) = \frac{A}{\sqrt{\gamma_{\text{eff}}}} e^{-S^{\text{OFF}}(t)} \left[e^{-S^{\text{ON}}(t_{\text{off}})} \int_0^{t_{\text{off}}} \frac{f_E^{\text{ON}}(t') e^{S^{\text{ON}}(t')}}{\sqrt{t-t'}} dt' + \int_{t_{\text{off}}}^t \frac{f_E^{\text{OFF}}(t') e^{S^{\text{OFF}}(t')}}{\sqrt{t-t'}} dt' \right]. \quad (\text{B6})$$

During the switching-off process, $\mu_j \tau_f \gg 1$, thus we can neglect the exponential term in Eq. (B5) so that $\exp[-S^{\text{OFF}}(t)] \approx \exp[-\frac{f_E^{\text{ON}}(t_{\text{off}})}{\gamma_{\text{eff}}} \sum_{j,j'=1}^2 \frac{b_j b_{j'}}{\mu_j + \mu_{j'}}] = g \approx 1$.

Therefore,

$$\delta \tilde{\varepsilon}_f^{\text{OFF}}(t > t_{\text{off}}) = \frac{A}{\sqrt{\gamma_{\text{eff}}}} \left[g f_0 e^{-a_1^2 t_{\text{off}} / \tau_f} \sum_{i,i'=1}^3 a_i a_{i'} \int_0^{t_{\text{off}}} \frac{e^{-\lambda_{ii'} t'}}{\sqrt{t-t'}} dt' + f_E^{\text{ON}}(t_{\text{off}}) \sum_{j,j'=1}^2 b_j b_{j'} \int_{t_{\text{off}}}^t \frac{e^{-(\mu_j + \mu_{j'})(t'-t_{\text{off}})}}{\sqrt{t-t'}} dt' \right]. \quad (\text{B7})$$

Representing the integrals in the first sum of Eq. (B7) as $\int_0^{t_{\text{off}}} dt' = \int_0^t dt' - \int_{t_{\text{off}}}^t dt'$ and using Eq. (B3), we obtain Eq. (40).

[1] P. G. de Gennes and J. Prost, *The Physics of Liquid Crystals* (Clarendon, Oxford, 1993).

[2] C. P. Fan and M. J. Stephen, *Phys. Rev. Lett.* **25**, 500 (1970).

- [3] P. Palffy-Muhoray and D. A. Dunmur, *Mol. Cryst. Liq. Cryst.* **97**, 337 (1983).
- [4] A. J. Nicastro and P. H. Keyes, *Phys. Rev. A* **30**, 3156 (1984).
- [5] E. F. Gramsbergen, L. Longa, and W. H. de Jeu, *Phys. Rep.* **135**, 195 (1986).
- [6] I. Lelidis, M. Nobili, and G. Durand, *Phys. Rev. E* **48**, 3818 (1993).
- [7] I. Lelidis and G. Durand, *Phys. Rev. E* **48**, 3822 (1993).
- [8] J. A. Olivares, S. Stojadinovic, T. Dingemans, S. Sprunt, and A. Jáklí, *Phys. Rev. E* **68**, 041704 (2003).
- [9] R. Stannarius, A. Eremin, M. G. Tamba, G. Pelzl, and W. Weissflog, *Phys. Rev. E* **76**, 061704 (2007).
- [10] M. Nagaraj, Y. P. Panarin, U. Manna, J. K. Vij, C. Keith, and C. Tschierske, *Appl. Phys. Lett.* **96**, 011106 (2010).
- [11] V. Borshch, S. V. Shiyanovskii, and O. D. Lavrentovich, *Mol. Cryst. Liq. Cryst.* **559**, 97 (2012).
- [12] V. Borshch, S. V. Shiyanovskii, and O. D. Lavrentovich, *Phys. Rev. Lett.* **111**, 107802 (2013).
- [13] B.-X. Li, V. Borshch, S. V. Shiyanovskii, S.-B. Liu, and O. D. Lavrentovich, *Appl. Phys. Lett.* **104**, 201105 (2014).
- [14] M. Kleman and O. D. Lavrentovich, *Soft Matter Physics: An Introduction* (Springer, New York, 2003).
- [15] P. G. de Gennes, *C. R. Acad. Sci. Paris, Ser. B* **266**, 15 (1968).
- [16] Groupe d'Etudes des Cristaux Liquides (Orsay), *J. Chem. Phys.* **51**, 816 (1969).
- [17] J. L. Martin and G. Durand, *Solid State Commun.* **10**, 815 (1972).
- [18] Y. Poggi and J. C. Filippini, *Phys. Rev. Lett.* **39**, 150 (1977).
- [19] T. E. Faber, *Proc. R. Soc. London, Ser. A* **353**, 247 (1977).
- [20] B. Malraison, Y. Poggi, and E. Guyon, *Phys. Rev. A* **21**, 1012 (1980).
- [21] M. Warner, *Mol. Phys.* **52**, 677 (1984).
- [22] A. Seppen, G. Maret, A. Jansen, P. Wyder, J. Janssen, and W. de Jeu, in *Biophysical Effects of Steady Magnetic Fields: Proceedings of the Workshop, Les Houches* (Springer, Berlin, 1986), p. 18.
- [23] D. A. Dunmur and P. Palffy-Muhoray, *J. Phys. Chem.* **92**, 1406 (1988).
- [24] T. E. Faber, *Liq. Cryst.* **9**, 95 (1991).
- [25] B. J. Gertner and K. Lindenberg, *J. Chem. Phys.* **94**, 5143 (1991).
- [26] M. J. Freiser, *Phys. Rev. Lett.* **24**, 1041 (1970).
- [27] J. P. Straley, *Phys. Rev. A* **10**, 1881 (1974).
- [28] C. Zannoni, in *The Molecular Physics of Liquid Crystals*, edited by G. R. Luckhurst and G. W. Gray (Academic, London/New York, 1979).
- [29] G. R. Luckhurst, *Liq. Cryst.* **36**, 1295 (2009).
- [30] D. A. Varshalovich, A. N. Moskalev, and V. K. Khersonskii, *Quantum Theory of Angular Momentum: Irreducible Tensors, Spherical Harmonics, Vector Coupling Coefficients, 3 Nj Symbols* (World Scientific, Singapore, 1988).
- [31] A. M. Sonnet, E. G. Virga, and G. E. Durand, *Phys. Rev. E* **67**, 061701 (2003).
- [32] S. V. Shiyanovskii, *Phys. Rev. E* **87**, 060502(R) (2013).
- [33] Y. Yin, S. V. Shiyanovskii, and O. D. Lavrentovich, *J. Appl. Phys.* **100**, 024906 (2006).
- [34] L. D. Landau and I. M. Khalatnikov, *Dokl. Akad. Nauk SSSR* **96**, 469 (1954) [*Collected Papers of L.D. Landau*, edited by D. Ter Haar (Pergamon Press, Oxford, 1965), p. 469].
- [35] S. Hess, *Z. Naturforsch. A* **31**, 1507 (1976).
- [36] P. D. Olmsted and P. M. Goldbart, *Phys. Rev. A* **46**, 4966 (1992).
- [37] R. Berardi, L. Muccioli, S. Orlandi, M. Ricci, and C. Zannoni, *J. Phys.: Condens. Matter* **20**, 463101 (2008).
- [38] S. V. Shiyanovskii, *Ukr. J. Phys.* **26**, 137 (1981).
- [39] B. Y. Zel'dovich and N. V. Tabiryan, *Zh. Eksp. Teor. Fiz.* **81**, 1738 (1981) [*Sov. Phys. JETP* **54**, 922 (1981)].
- [40] M. Abramowitz and I. A. Stegun, *Handbook of Mathematical Functions: With Formulas, Graphs, and Mathematical Tables* (Dover, New York, 1964).
- [41] R. N. Thurston, G. D. Boyd, and D. C. Senft, *J. Appl. Phys.* **55**, 3846 (1984).
- [42] H. G. Walton, *Mol. Cryst. Liq. Cryst.* **574**, 60 (2013).
- [43] B. S. Scheuble, G. Weber, and R. Eidenschink, *Proc. Eurodisplay* **84**, Paris, 65 (1984).
- [44] U. Krüger, R. Pepperl, and U. J. Schmidt, *Proc. IEEE* **61**, 992 (1973).
- [45] M. Beevers and G. Khanarian, *Aust. J. Chem.* **32**, 263 (1979).
- [46] J. M. Neto and A. B. Villaverde, *J. Phys.: Condens. Matter* **8**, 2791 (1996).
- [47] P. G. de Gennes, *Phys. Lett. A* **30**, 454 (1969).
- [48] A. R. Johnston, *J. Appl. Phys.* **44**, 2971 (1973).
- [49] J. C. Filippini and Y. Poggi, *J. Phys. Lett.* **35**, 99 (1974).
- [50] M. Schadt, *J. Chem. Phys.* **67**, 210 (1977).
- [51] L. Schneider and J. H. Wendorff, *Liq. Cryst.* **22**, 29 (1997).
- [52] H. Khoshshima, H. Tajalli, A. G. Gilani, and R. Dabrowski, *J. Phys. D* **39**, 1495 (2006).
- [53] G. R. Luckhurst, *Thin Solid Films* **393**, 40 (2001).